Dynamic seismic ruptures on melting fault zones

Andrea Bizzarri[1]

Received 25 May 2010; revised 24 November 2010; accepted 17 December 2010; published 19 February 2011.

[1] We present a physical model that describes the behavior of spontaneous earthquake ruptures dynamically propagating on a fault zone and that accounts for the presence of frictional melt produced by the sliding surfaces. First, we analytically derive the solution for the temperature evolution inside the melt layer, which generalizes previous approximations. Then we incorporate such a solution into a numerical code for the solution of the elastodynamic problem. When a melt layer is formed, the linear slip-weakening law (initially governing the fault and relying on the Coulomb friction) is no longer valid. Therefore we introduce on the fault a linearly viscous rheology, with a temperature-dependent dynamic viscosity. We explore through numerical simulations the resulting behavior of the traction evolution in the cohesive zone before and after the transition from Coulomb friction and viscous rheology. The predictions of our model are in general agreement with the data from exhumed faults. We also find that the fault, after undergoing the breakdown stress drop controlled by the slip-weakening constitutive equation, experiences a second traction drop controlled by the exponential weakening of fault resistance due to the viscous rheology. This further drop enhances the instability of the fault, increasing the rupture speeds, the peaks in fault slip velocity, and the fracture energy density.

Citation: Bizzarri, A. (2011), Dynamic seismic ruptures on melting fault zones, *J. Geophys. Res.*, *116*, B02310, doi:10.1029/2010JB007724.

1. Introduction

[2] The melting process is a phase change of a substance from its solid state to the liquid state. The application of pressure or heat causes the internal energy of the substance to increase, resulting in a temperature rise up to the melting point, at which the solid undergoes to a less-ordered state (liquid phase).

[3] Ice melting is familiar in skiing and it has recently considered a possible cause of Arctic warming [*Screen and Simmonds*, 2010]. In rock mechanics it is now clear that the most of the energy dissipated on a seismogenic fault is ultimately converted into frictional heat [e.g., *Pittarello et al.*, 2008] and that the temperature increase (ΔT) due to seismic slip can exceed the melting temperature of crustal rocks.

[4] Although rare field evidence for melting on exhumed faults engenders skepticism for the relevance of melt during earthquakes [*Rempel and Rice*, 2006], partial melting at local asperity contacts can occur [*Jeffreys*, 1942; *McKenzie and Brune*, 1972] and a continuous macroscopic melt layer may be present after some cosesimic slip.

[5] Indeed, large temperature increases leading to melting have been already obtained in dynamic models of spontaneously spreading earthquake ruptures obeying different fault governing laws. It has been found in numerical models that, for localized shear, both the thermal pressurization of pore fluids [*Bizzarri and Cocco*, 2006a, 2006b] (hereinafter referred to as BC06a and BC06b, respectively) and the flash heating of microasperity contacts [*Bizzarri*, 2009] do not reduce the frictional resistance on the fault surface enough to prevent melting. To date, the only possible exception [*Bizzarri*, 2010c] is represented by a slip- and velocity-dependent friction law, recently derived in high-velocity laboratory experiments by *Sone and Shimamoto* [2009].

[6] On the other hand, evidence of melting has also been found in laboratory experiments, when conditions similar to those typical of seismic deformation are attained [e.g., *Spray*, 1995; *Tsutsumi and Shimamoto*, 1997; *Hirose and Shimamoto*, 2003].

[7] When a continuous film of molten material is formed within the fault structure (see section 5.3), the "classical" governing models, essentially derived within the Coulomb-Amonton-Mohr framework, are no longer valid, since the coseismic increase in temperature affects the frictional properties of rocks [e.g., *Sibson*, 1977; *Lachenbruch*, 1980].

[8] The main goal of the present paper is to extend previous spontaneous dynamic rupture models and to account also for non-Coulombian rheology of a fault. We will develop a physical model which, under some assumptions, incorporates the melt behavior (via a Newtonian rheology of a temperature-dependent viscous fluid). The present study also aims to extend previous papers [*Nielsen et al.*, 2008, 2010], where a constant sliding velocity was assumed and where only the behavior after the onset of melting was

[1]Sezione di Bologna, Istituto Nazionale di Geofisica e Vulcanologia, Bologna, Italy.

0148-0227/11/2010JB007724

explored. On the contrary, we account here for the transition from the "classical" behavior of rocks before melting to the viscous behavior after the formation of a melt layer.

[9] The paper is organized as follows: In section 2 we will describe the adopted fault model. The temperature evolution before the melting point is briefly summarized in section 3, while in section 4 we derive the time evolution of the temperature in the molten region (analytical details and comparisons with previous solutions are discussed in the appendixes). In section 5 we introduce the fault rheology (i.e., the fault boundary condition expressing the governing law). Section 6 is devoted to the introduction of the two-state physics (Stefan problem). The results of the numerical experiments on synthetic earthquakes, for a special case of melt layer evolution, are presented and discussed in sections 7 and 8. Section 9 discusses the shape of the melt layer, while section 10 summarizes the prominent conclusions of the present study.

2. Model of the Fault Zone and Statement of the Problem

[10] In the present paper we consider a more general fault structure than that adopted by BC06a and BC06b [see also *Evans and Chester*, 1995; *Sibson*, 2003; *Bizzarri*, 2010a]. As reported in Figure 1, a highly fractured, damage zone surrounds the slipping zone where the slip is concentrated. The latter can be regarded to represent the fault core, the ultracataclastic shear zone or the gouge layer. For simplicity, we assume here that the slipping zone has a thickness $2w$, which is spatially homogeneous along the strike and the dip directions of the fault. The boundaries between the slipping zone and the damage zone are perpendicular to the normal fault coordinate, ζ, which has its origin in the middle of the slipping zone. The plane $\zeta = 0$ can be associated with the principal slipping zone and can be regarded as the mathematical idealization of the fault surface (or fault plane) where the dynamic variables, such as traction, velocity, etc., are formally defined.

[11] Depending on the rupture dynamics, the frictional heat can be such that melting is produced. As a consequence a melt layer having thickness equal to $2w_m$ can also exist within the slipping zone of width $2w$ (Figure 1). By definition, melting occurs in a specific point if the temperature at that point exceeds the melting temperature, T_m. The resulting melt layer is also centered at $\zeta = 0$. This assumption is physically reasonable, since we consider spatially homogeneous properties within $2w$ (i.e., we neglect the chemical complexity of the minerals) and we know that in this case the maximum temperature is developed in the middle of the slipping zone (let us say, on the mathematical fault plane) and decreases for increasing off-fault distances [*Andrews*, 2002; BC06a]. The thickness of melt layer increases through time, depending on the temperature evolution within $2w$, and its rate of increase, $(\mathrm{d}/\mathrm{d}t)w_m(t) \equiv \dot{w}_m(t)$, in full of generality can be variable through time. In the remainder of the paper, we will denote the left and right boundaries separating the solid and the melted rocks as $\zeta = -w_m(t)$ and $\zeta = w_m(t)$, respectively. These quantities, as well as $\dot{w}_m(t)$, are a priori unknown.

[12] Since we presently do not have enough observational constrains to physically describe the physics of the damage zone, where elastoplastic processes are expected to take place, in the model we will consider times up to the time level at which the whole slipping zone has molten; that is, we prescribe that $w_m \le w$. In other words, we do not allow for the melting of the damage zone. Moreover, we do not account in the present model the melt removal by extrusion outside the slipping zone, through the so-called injection veins [*Sibson*, 1975].

[13] In the following, for brevity of notation, we will omit the explicit dependence on the on-fault coordinates ξ_1 and ξ_3 while we only put the possible dependence on ζ. We will denote with the symbol $\breve{\bullet}$ the quantities pertaining to the melt layer and with t_m the time instant when melting starts locally (i.e., at asperity contacts level). Time t_m is formally defined by the following condition:

$$t_m \text{ such that } T^f(t_m) \equiv T(\zeta = 0, t = t_m) = T_m. \tag{1}$$

Also t_m is a priori unknown since it depends on the rupture dynamics (which in turn controls the temperature evolution, $T(\zeta, t)$, within the slipping zone).

[14] Finally, in the following analysis we will assume that thermal pressurization is unimportant (i.e., we assume perfectly drained configurations) and other weakening mechanisms are not operating. Of course, the inclusion of pore pressure variation can alter the dynamics of the fault [*Andrews*, 2002; BC06b] and ultimately the temperature developed by frictional heat.

3. Temperature Evolution Before the Melting Time

[15] For times $t < t_m$ the whole slipping zone thickness is composed only by material (rocks, gouge,…) in the solid state; the temperature evolution is the solution of the heat conduction equation:

$$\frac{\partial}{\partial t} T(\zeta, t) = \chi \frac{\partial^2}{\partial \zeta^2} T(\zeta, t) + \frac{1}{c} q(\zeta, t) \tag{2}$$

where χ is the thermal diffusivity of the material in its solid state ($\chi = \kappa/\rho C_p$, where κ is the thermal conductivity), assumed to be uniform along ζ, $c \equiv \rho C_p$ is the heat capacity for unit volume of the bulk composite (ρ being the cubic mass density of the composite and C_p its specific heat at constant pressure), and q is the heat generated for unit volume and for unit time ($[q] = \mathrm{J/(m^3\ s)} = \mathrm{W/m^3}$). Physically, χ expresses the ability of a substance to adjust its temperature to that of its surroundings (materials with a high value of χ conduct the heat quickly, compared to their volumetric heat, and therefore they rapidly adjust their temperature). q represents the heat source due to frictional heat and its integral over the coordinate ζ gives the heat flux (i.e., the heat produced per unit area on the fault and per unit time). Equation (2) has the exact solution (see BC06a, their equation (A4)):

$$T(\zeta, t) = T_0 + \frac{1}{4cw} \int_0^{t-\varepsilon} \mathrm{d}t' \left\{ \mathrm{erf}\left(\frac{\zeta + w}{2\sqrt{\chi(t - t')}} \right) - \mathrm{erf}\left(\frac{\zeta - w}{2\sqrt{\chi(t - t')}} \right) \right\} \tau(t') v(t'), \tag{3}$$

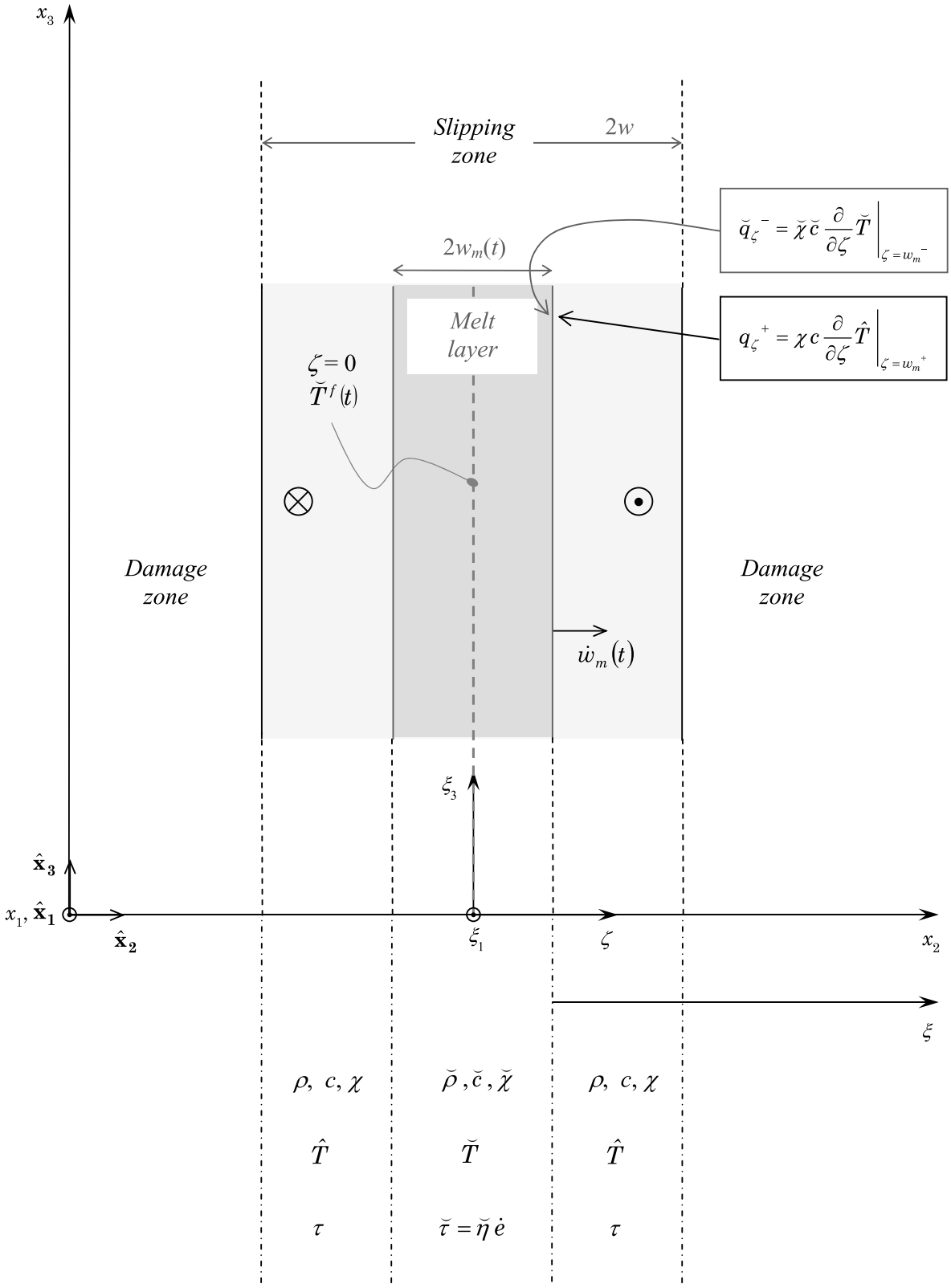

Figure 1. Sketch representing the considered fault structure. At a generic time after the onset of melting, a melt layer of thickness $2w_m(t)$ and enlarging with rate $\dot{w}_m(t)$ exists within a slipping zone $2w$ thick. The latter is surrounded by the damage zone. The plane $\zeta = 0$ defines, in the Cartesian reference system $O\xi_1\zeta\xi_3$, the center of the slipping zone (i.e., the idealized fault plane). The coordinate ξ is normal to the fault plane and is anchored to the melt-solid boundary ($\xi \equiv \zeta - w_m(t)$).

where T_0 is the initial temperature distribution (i.e., $T_0 \equiv T_0(\zeta, 0)$), erf( ) is the error function

$$\left(\mathrm{erf}(z) \underset{\mathrm{df}}{=} \frac{2}{\sqrt{\pi}} \int_0^z \mathrm{d}x\, \mathrm{e}^{-x^2}\right),$$

$2w$ is the thickness of the slipping zone, and ε is an arbitrarily small positive real number (see BC06a for further details). We assume here that $2w$ is spatially homogeneous and constant through time, although temporal variations in the slipping zone thickness can have relevant effects in the time scale of the seismic cycle of the fault [*Bizzarri*, 2010e]. In equation (3), v denotes the magnitude of the fault slip velocity and τ denotes the magnitude of the fault traction, expressed by the governing law in the unmelted regime, which can be the slip-weakening law [e.g., *Ida*, 1972], a rate- and state-dependent friction law [e.g., *Dieterich*, 1979], the law for the flash heating of microasperity contacts [*Noda et al.*, 2009, and references therein], etc. (see *Bizzarri* [2010a] for a discussion). On the fault plane (i.e., in the limit $\zeta = 0$), equation (3) reduces to (see also BC06a, their equation (6)):

$$T^f(t) \equiv T(0,t) = T_0^f + \frac{1}{2cw} \int_0^{t-\varepsilon} \mathrm{d}t'\, \mathrm{erf}\left(\frac{w}{2\sqrt{\chi(t-t')}}\right) \tau(t')v(t'), \tag{4}$$

where $T_0^f \equiv T(0,0)$, that is, the initial temperature distribution on the fault plane. We simply recall here that solutions (3) and (4) pertain to the heat source

$$q(\zeta,t) = \begin{cases} \dfrac{\tau(t)v(t)}{2w} & ,t>0, |\zeta| \le w \\ 0 & ,|\zeta| > w \end{cases}, \tag{5}$$

which implicitly assumes that all the work spent to allow the fault sliding is converted into heat [see also *Fialko*, 2004; BC06a; BC06b; *Pittarello et al.*, 2008; *Bizzarri*, 2009].

4. Temperature Evolution After the Melting Point: Behavior Inside the Melt Layer

[16] After the melting point t_m we have a phase transition (from solid to molten materials) and therefore we have to consider a Stefan-like problem, accounting for two-state physics (see section 6). Here we will focus on the behavior of the temperature field inside the molten region. Specifically, we have to solve the following PDE:

$$\frac{\partial}{\partial t} \breve{T}(\zeta,t) = \breve{\chi} \frac{\partial^2}{\partial \zeta^2} \breve{T}(\zeta,t) + \frac{\mathrm{d}}{\mathrm{d}t} w_m(t) \frac{\partial}{\partial \zeta} \breve{T}(\zeta,t) + \frac{1}{\breve{c}} \breve{q}(\zeta,t). \tag{6}$$

As discussed in detail by *Nielsen et al.* [2010], the term on the left-hand side of equation (6) and the diffusion term

$$\frac{\mathrm{d}}{\mathrm{d}t} w_m(t) \frac{\partial}{\partial \zeta} \breve{T}(\zeta,t)$$

can be neglected because they are dominated by the heat source term

$$\frac{1}{\breve{c}} \breve{q}(\zeta,t)$$

(as also checked numerically in Appendix B). Consequently, we have to solve the approximated equation

$$\breve{\chi} \frac{\partial^2}{\partial \zeta^2} \breve{T}(\zeta,t) = -\frac{1}{\breve{c}} \breve{q}(\zeta,t), \tag{7}$$

where $|\zeta| \le w_m(t)$ and $t \ge t_m$. Let now consider the elementary, nonsingular, heat source function:

$$\breve{q}^{el}(\zeta,t) = \frac{h\, \mathrm{e}^{-\frac{\zeta^2}{2w_m^2(t)}}}{\sqrt{2\pi} w_m(t)} \Theta(t-t_m), \tag{8}$$

which has been frequently employed in the literature [e.g., *Andrews*, 2002; *Noda et al.*, 2009] and assumes that the inelastic strain is distributed as a Gaussian in the distance ζ, with a standard deviation equal to the half thickness of the melt layer (so that 68% of the deformation occurs in a thickness of $2w_m$). In equation (8), Θ( ) is the Heaviside step function and $[h]$ = Pa/(m s), so that $[\breve{q}^{el}]$ = Pa/s. The elementary problem is completed by the boundary conditions:

$$\begin{matrix} \breve{T}(\zeta = -w_m(t), t) = T_m \\ \breve{T}(\zeta = w_m(t), t) = T_m, \end{matrix} \quad ,\forall\ t\ \ge\ t_m. \tag{9}$$

The elementary problem (equations (7) with (8)) has the following solution:

$$\breve{T}^{el}(\zeta,t) = C_1 + C_2\zeta - h \frac{\zeta\, \mathrm{erf}\left(\dfrac{\zeta}{\sqrt{2}w_m(t)}\right) + \sqrt{\dfrac{2}{\pi}}\, \mathrm{e}^{-\frac{\zeta^2}{2w_m^2(t)}} w_m(t)}{2\, \breve{c}\breve{\chi}} \tag{10}$$

with $t \ge t_m$. Note that, formally, the time dependence in $\breve{T}^{el}$ is implicit (it is due to time variability of w_m). In equation (10) the two constants of integration C_1 and C_2 are determined by considering the boundary conditions in equation (9) that lead to

$$\breve{T}^{el}(\zeta,t) = T_m - h \frac{\zeta\, \mathrm{erf}\left(\dfrac{\zeta}{\sqrt{2}w_m(t)}\right)}{2\, \breve{c}\breve{\chi}} + h \frac{\left(\sqrt{\dfrac{2\pi}{\mathrm{e}}} + \pi\, \mathrm{erf}\left(\dfrac{1}{\sqrt{2}}\right) - \sqrt{2\pi}\, \mathrm{e}^{-\frac{\zeta^2}{2w_m(t)^2}}\right) w_m(t)}{2\pi\, \breve{c}\breve{\chi}} \tag{11}$$

where again $t \geq t_m$. Simple algebra shows that equation (11) satisfies both conditions in equation (9), for arbitrary value of half-layer thickness (or in other words for all arbitrary times $t \geq t_m$). We remark that the solution (11) depends on $w_m(t)$, which is still unknown; here we simply note that we have the following condition for $w_m(t)$:

$$w_m(t) = 0, \ \forall \ t \leq t_m, \tag{12}$$

stating the obvious fact that the thickness of the melt layer is null at the melting instant and does not exist before that time.

[17] Let now we consider the heat input $h = \breve{\tau}(\zeta, t)\, v(t)$; this gives the actual heat source:

$$\breve{q}(\zeta, t) = \frac{\breve{\tau}(\zeta, t)\, v(t)\, \mathrm{e}^{-\frac{\zeta^2}{2w_m^2(t)}}}{\sqrt{2\pi} w_m(t)} \Theta(t - t_m). \tag{13}$$

In equation (13), $\breve{\tau}(\zeta, t)$ is the traction when $t \geq t_m$, which is described with more details in section 5. By using equation (13), the general evolution of the temperature inside the melt layer can be expressed as follows:

$$\breve{T}(\zeta, t) = T_m - \left[\frac{\zeta \operatorname{erf}\left(\frac{\zeta}{\sqrt{2} w_m(t)} \right)}{2\, \breve{c}\, \breve{\chi}} - \frac{\left(\sqrt{\frac{2\pi}{\mathrm{e}}} + \pi \operatorname{erf}\left(\frac{1}{\sqrt{2}} \right) - \sqrt{2\pi}\, \mathrm{e}^{-\frac{\zeta^2}{2w_m^2(t)}} \right) w_m(t)}{2\pi\, \breve{c}\, \breve{\chi}} \right] \cdot \breve{\tau}(\zeta, t) v(t), \tag{14}$$

where again $t \geq t_m$. Interestingly, we can note that at $t = t_m$ the second term inside the square brackets vanishes (because of equation (12)), as does the first term too (we recall that equation (14) holds for ζ in the interval $[-w_m(t), w_m(t)]$, which at $t = t_m$ simply reduces to $\zeta = 0$), so that $\breve{T}(0, t_m) \equiv \breve{T}^f(t_m) = T_m$, in agreement with equation (1).

[18] In the limit $\zeta = 0$ (exploiting again the condition (12)), equation (14) can be written as

$$\breve{T}^f(t) \equiv \breve{T}(0, t) = T_m + \frac{\left(\sqrt{\frac{2\pi}{\mathrm{e}}} + \pi \operatorname{erf}\left(\frac{1}{\sqrt{2}} \right) - \sqrt{2\pi} \right)}{2\pi\, \breve{c}\, \breve{\chi}} \cdot \Theta(t - t_m) w_m(t)\, \breve{\tau}\, (t) v(t). \tag{15}$$

5. Fault Rheology

5.1. Coulomb Friction Before Melting

[19] In sections 3 and 4 we have invoked the shear traction τ for the phase prior to melting (section 3) and $\breve{\tau}$ after the melting instant (t_m). In this section we will discuss in more details how to incorporate the fault rheology (i.e., the fault governing law) in our dynamic model.

[20] For $t < t_m$ the quantity τ is expressed by one of the "classical" friction laws based on the Amonton-Coulomb-Mohr theory, stating a linear proportionality between τ and effective normal stress σ_n^{eff}, through the friction coefficient μ ($\tau = \mu \sigma_n^{eff}$). For simplicity and to better understand the effects of the presence of melting we adopt here the widely adopted linear slip-weakening (SW henceforth) constitutive relation, recalled here for convenience:

$$\tau^{(\mathrm{SW})} = \begin{cases} \tau_u - (\tau_u - \tau_f) \dfrac{u}{d_0} & , \ u < d_0 \\ \tau_f & , \ u \geq d_0 \end{cases}, \tag{16}$$

where τ_u defines the upper yield stress ($\tau_u = \mu_u \sigma_n^{eff}$), τ_f defines the upper kinetic stress ($\tau_f = \mu_f \sigma_n^{eff}$), and d_0 is the characteristic SW distance, quantifying the amount of cumulative slip required to complete the breakdown process (i.e., the stress release).

5.2. Governing Law for a Continuous Melt Layer

[21] In the presence of melting the relation $\tau = \mu \sigma_n^{eff}$ is no longer valid, owing to a more complex coupling between traction and normal stress. *Nielsen et al.* [2008, equation (57)] found an approximate behavior for $\breve{\tau}$ at high slip rates (namely, for

$$v \gg W \equiv \sqrt{\frac{8 \breve{T}_c \breve{\chi} \breve{c}}{\breve{\eta}_c}}$$

which is nearly equal to 0.4 m/s for typical parameters; see Table 1). However, this approximation holds only in the special case of steady state motion, and not in the case of variable slip velocity as in spontaneous rupture models.

[22] Following *Fialko* [2004], in a molten film of width $2w_m$ most of the resistance to slip comes from viscous deformation of the molten layer. By assuming a Newtonian fluid, postulating a linear dependence between the applied stress and the resulting rate of shear strain $\dot{e}$, we have

$$\tau^{(\mathrm{NF})} = \breve{\eta}\, \breve{\dot{e}}, \tag{17}$$

where $\breve{\eta}$ is the dynamic viscosity of the melt material ($\breve{\eta} = \breve{\eta}(\zeta, t)$; note that the dependence of $\breve{\eta}$ on ζ and t is implicit, since $\breve{\eta} = \breve{\eta}(\breve{T})$ and $\breve{T}$ depends on ζ and t). Several studies [e.g., *Shaw*, 1972; *Dingwell*, 1998] indicate that the temperature dependence of viscosity can be satisfactorily described by the Arrhenius law:

$$\breve{\eta}(\zeta, t) = \breve{K}\, \mathrm{e}^{\frac{\breve{T}_a}{\breve{T}(\zeta, t - \varepsilon) + 273.15}}, \tag{18}$$

where $\breve{K}$ is an empirical constant ($[\breve{K}]$ = Pa s) and $\breve{T}_a$ is the activation temperature ($\breve{T}_a = \breve{E}_a / R$, being $\breve{E}_a$ the activation energy and R the universal gas constant [see also *Fialko and Khazan*, 2005]). Both the constants $\breve{K}$ and $\breve{T}_a$ depend on the rock composition. In equation (18) the temperature has to

Table 1. Parameters Adopted in the Present Study[a]

Parameter	Value
Medium and Discretization Parameters	
Lamé constants, $\lambda = G$	35.9 GPa
S wave velocity, v_S	3.464 km/s
P wave velocity, v_P	6 km/s
Fault length, L^f	16 km
Fault width, W^f	11.6 km
Spatial grid size, $\Delta x_1 = \Delta x_2 = \Delta x_3 \equiv \Delta x$	25 m
Time step, Δt	6×10^{-4} s[b]
Constitutive Parameters	
Effective normal stress, σ_n^{eff}	120 MPa
Initial shear stress (prestress), τ_0	73.8 MPa
Upper yield stress, τ_u	81.24 MPa
Kinetic friction level, τ_f	55.2 MPa[c]
Characteristic slip-weakening distance, d_0	0.4 m
Thermal Parameters	
Initial temperature in the center of the slipping zone, T_0^f	210°C
Melting temperature, T_m	1200°C[d]
Latent heat of fusion, L	350×10^3 J/kg
Slipping zone thickness (reference), $2w$	2 mm

Thermal Parameter	Value: Solid State	Value: Molten State
Cubic mass density, ρ or $\breve{\rho}$[e]	2990 kg/m^3	2591 kg/m^3
Heat capacity for unit volume of the composite, c or $\breve{c}$[e]	2.838×10^6 J/(m^3 °C)	3.845×10^6 J/(m^3 °C)
Thermal diffusivity, χ or $\breve{\chi}$[e]	0.344×10^{-6} m^2/s	0.8×10^{-6} m^2/s
Arrhenious constant, $\breve{K}$	n/a	145.37 Pa s[f]
Activation temperature, $\breve{T}_a$	n/a	6233 K[d]

[a]Parameters refer to gabbro.

[b]For the adopted parameters, the Courant-Friedrichs-Lewy ratio, $\omega_{CFL} \underset{\text{df}}{=} v_S \Delta t/\Delta x$, equals 0.083, and the estimate of the critical frequency for spatial grid dispersion, $f_{acc}^{(s)} = v_S/(6\Delta x)$, equals 23 Hz.

[c]This results in a strength parameter $S = 0.4$ ($S \underset{\text{df}}{=} (\tau_u - \tau_0)/(\tau_0 - \tau_f)$).

[d]As in the work of *Nielsen et al.* [2008], we assume a single value of T_m even if each mineral composing the material assemblage in the slipping zone can have a different melting temperature, leading to martial melts and polyphases [see *Spray*, 1992].

[e]Extrapolation from *Holland and Powell* [1990]; for the solid state, we assume an average temperature between T_0^f and T_m.

[f]With these values of $\breve{K}$ and $\breve{T}_a$, we obtain the dynamic viscosity at melting point $\breve{\eta}_m \equiv \breve{\eta}(\breve{T} = T_m) = \breve{K}\, e^{\breve{T}_a/(T_m + 273.15)} = 1 \times 10^4$ Pa s (as in the work of *Nielsen et al.* [2008]).

be expressed in K (as $\breve{T}_a$) so we apply to $\breve{T}$ the usual shift (because $[T]$ = °C). Moreover, we note that in equation (18) the melting temperature is computed at the previous time level and therefore it enters into the heat source (equation (13)) as a known quantity. We will discuss in more details this approximation in Appendix C. On the other hand, we can express the deformation rate in the limit $\zeta = 0$ as

$$\breve{\dot{e}} = \frac{v}{2w_m}, \tag{19}$$

so that equation (17) becomes [see also *Fialko*, 2004]

$$\tau^{(\mathrm{NF})} = \breve{\eta}\,\frac{v}{2w_m}. \tag{20}$$

[23] Finally, on the fault plane, by combining equations (20) and (18), we obtain

$$\tau^{(\mathrm{NF})}(t) = \breve{K}\, e^{\frac{\breve{T}_a}{\breve{T}^f(t-\varepsilon) + 273.15}}\frac{v(t)}{2w_m(t)}, \tag{21}$$

where $\breve{T}^f$ is given by equation (15). In the limit of isoviscous melt (i.e., if we neglect the temperature dependence of viscosity), we will simply have

$$\tau^{(\mathrm{NF})}(t) = \breve{\eta}_m \frac{v(t)}{2w_m(t)}, \tag{22}$$

where

$$\breve{\eta}_m \equiv \breve{\eta}\left(\breve{T} = T_m\right) = \breve{K}\, e^{\frac{\breve{T}_a}{T_m + 273.15}}$$

is the reference dynamic viscosity at the melting point. Equations (20) and (22) can be regarded as the simplest case of a viscous fault rheology, which in general can be expressed as $\tau^n = v\alpha_n$, where n is a constant and α_n effectively controls the strength of the fault [see also *Hetland et al.*, 2010]; when $n = 1$ (linear viscous rheology), $\alpha_1 = \breve{\eta}/(2w_m)$.

5.3. Transition From Frictional Resistance to Viscous Shear

[24] First we notice that the frictional resistance $\tau^{(\mathrm{NF})}$ given by equation (21) (or by equation (22)) for small values of w_m can be greater than the average Coulomb-Mohr failure stress for the upper crust and greater than $\tau^{(\mathrm{SW})}$ expressed by

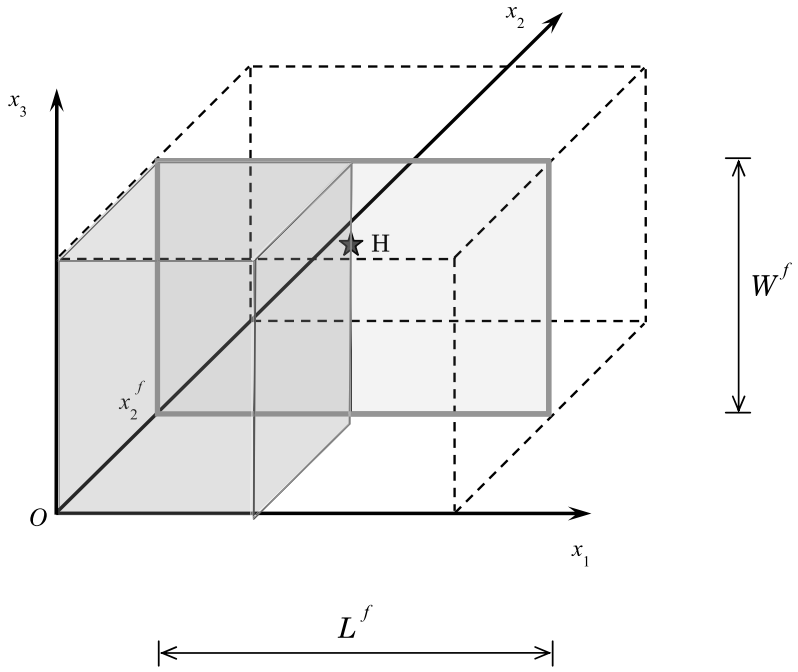

Figure 2. Geometry of the model. The light gray plane indicates the fault $x_2 = x_2^f$, while the gray box marks the portion of the computational domain where the calculations are performed, owing to the exploitation of the symmetry about the hypocenter H and about the fault plane (see *Bizzarri* [2009] for details).

equation (16). This would imply that, immediately after t_m, the fault will experience a significant increase of resistance to slip, which in turn can stop the ongoing rupture. Indeed, experiments by *Tsutsumi and Shimamoto* [1997] suggest that viscous braking might result after melting. Moreover, when the onset of melting is accompanied by increases in shear stress exceeding the static friction, or the intrinsic rock strength, the fused fault may be abandoned, and the slip may be transferred to a new subparallel plane [e.g., *Swanson*, 1992; *Otsuki et al.*, 2003]. As a consequence, it is possible than viscous braking causes the formation of multiple melt layers. These phenomena still require further observational constraints and we are not able to fully include them in the model. Therefore we make the conservative assumption that, after t_m, $\breve{\tau}$ is still described by Coulomb friction until the melt layer is sufficiently thick ($w_m = w_{m_c}$), so that $\tau^{(\mathrm{NF})}$ is lower (dominant) with respect to the Coulomb friction. This condition physically defines the formation of a continuous melt layer (having an initial width of $2w_{m_c}$). The macroscopic, continuous melt layer trapped between the fault walls, as opposed to microscopic melting occurring at asperity contacts level (at time t_m), would take place after some cosesimic slip. In many field observations this continuous layer can be absent owing to processes such as melt extrusion, not considered here.

[25] By considering that $\breve{\tau}$ still follows a Coulomb friction until $w_m = w_{m_c}$ we guarantee a continuous spreading of the propagating rupture; we also define an effective melting time t_m^{eff}, at which temperature exceeds an effective melting temperature $T_m^{eff} > T_m$:

$$T_m^{eff} \equiv T^f\left(t_m^{eff}\right) = T\left(0, t_m^{eff}\right) \text{ such that } \tau^{(\mathrm{NF})}\left(t_m^{eff}\right) < \tau^{(\mathrm{SW})}\left(t_m^{eff}\right). \tag{23}$$

[26] Practically, provided that $w_m(t)$ is determined (see sections 6, 7, and 8), we evaluate the fault temperature as follows:

$$\begin{cases} T = T_0^f + \dfrac{1}{2c\rho w}\displaystyle\int_0^{t-\varepsilon} \mathrm{d}t' \,\mathrm{erf}\left(\dfrac{w}{2\sqrt{\chi(t-t')}}\right)\tau(t')v(t') & ,\ t < t_m, \tau = \tau^{(\mathrm{SW})} \\ \breve{T} = T_m + \dfrac{\left(\sqrt{\dfrac{2\pi}{\mathrm{e}}} + \pi\,\mathrm{erf}\left(\dfrac{1}{\sqrt{2}}\right) - \sqrt{2\pi}\right)}{2\pi\,\breve{c}\breve{\rho}\breve{\chi}} w_m(t)\,\breve{\tau}\,(t)v(t) & ,\ t \geq t_m, \breve{\tau} = \mathrm{Min}\left\{\tau^{(\mathrm{SW})}, \tau^{(\mathrm{NF})}\right\} \end{cases} \tag{24}$$

with $\tau^{(\mathrm{SW})}$ as in equation (16) and $\tau^{(\mathrm{NF})}$ as in equation (21) or equation (22).

[27] We finally note that the adoption of the SW law enables us to identify the time instant when viscous shear

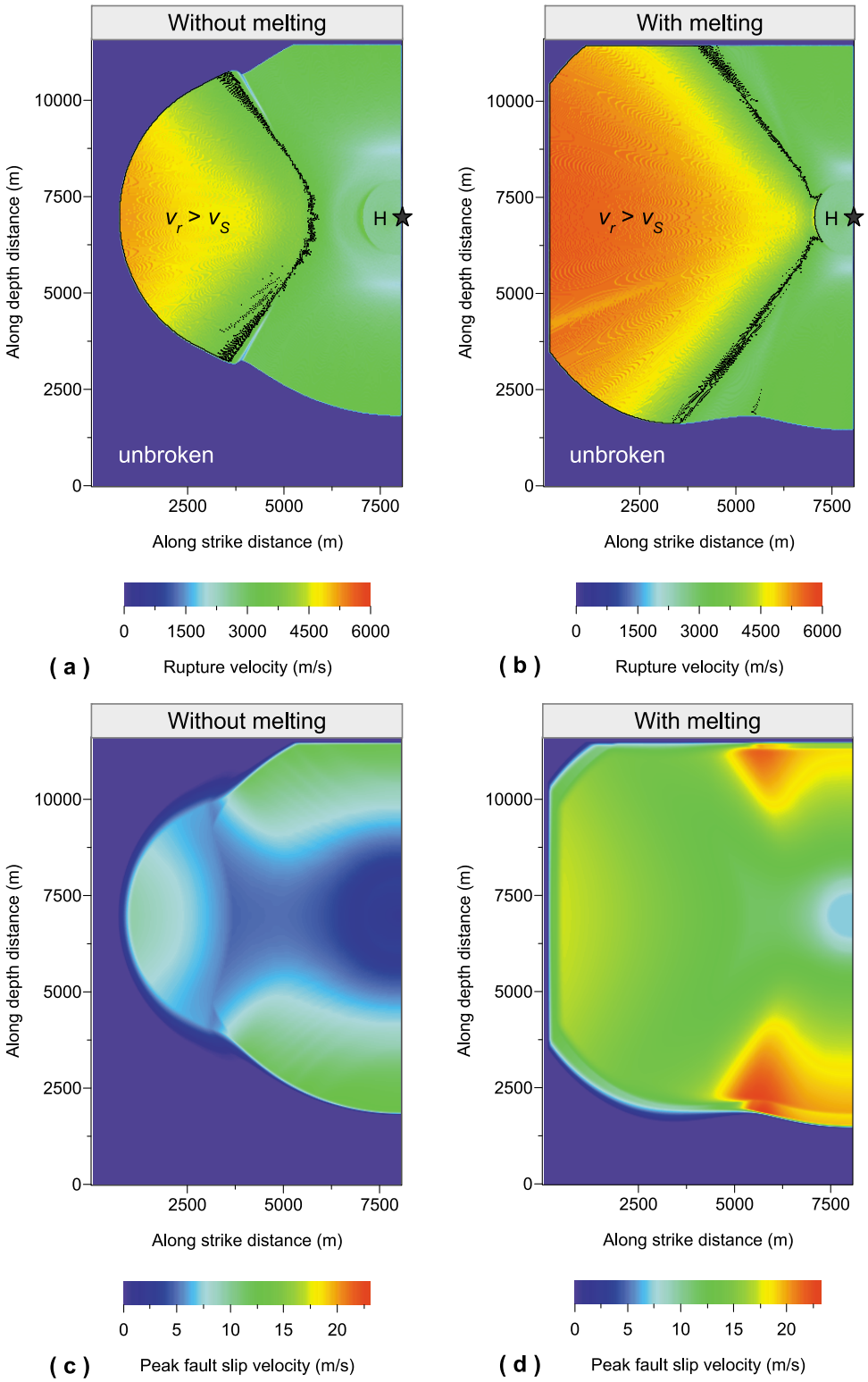

Figure 3. Comparison between results (a and c) neglecting melting and viscous shear and (b and d) considering melting and viscous shear. Figures 3a and 3b report the distribution of the rupture velocity (v_r) on the fault plane (v_r is the inverse of rupture time gradient). Figures 3c and 3d report the maximum (peak) fault slip velocity. The model without melting effects assumes a linear SW friction law (equation (16)), while the rheology of the model with melting is described in detail in sections 5.2 and 5.3. The adopted parameters are those tabulated in Table 1, and the melt layer evolves as in equation (27).

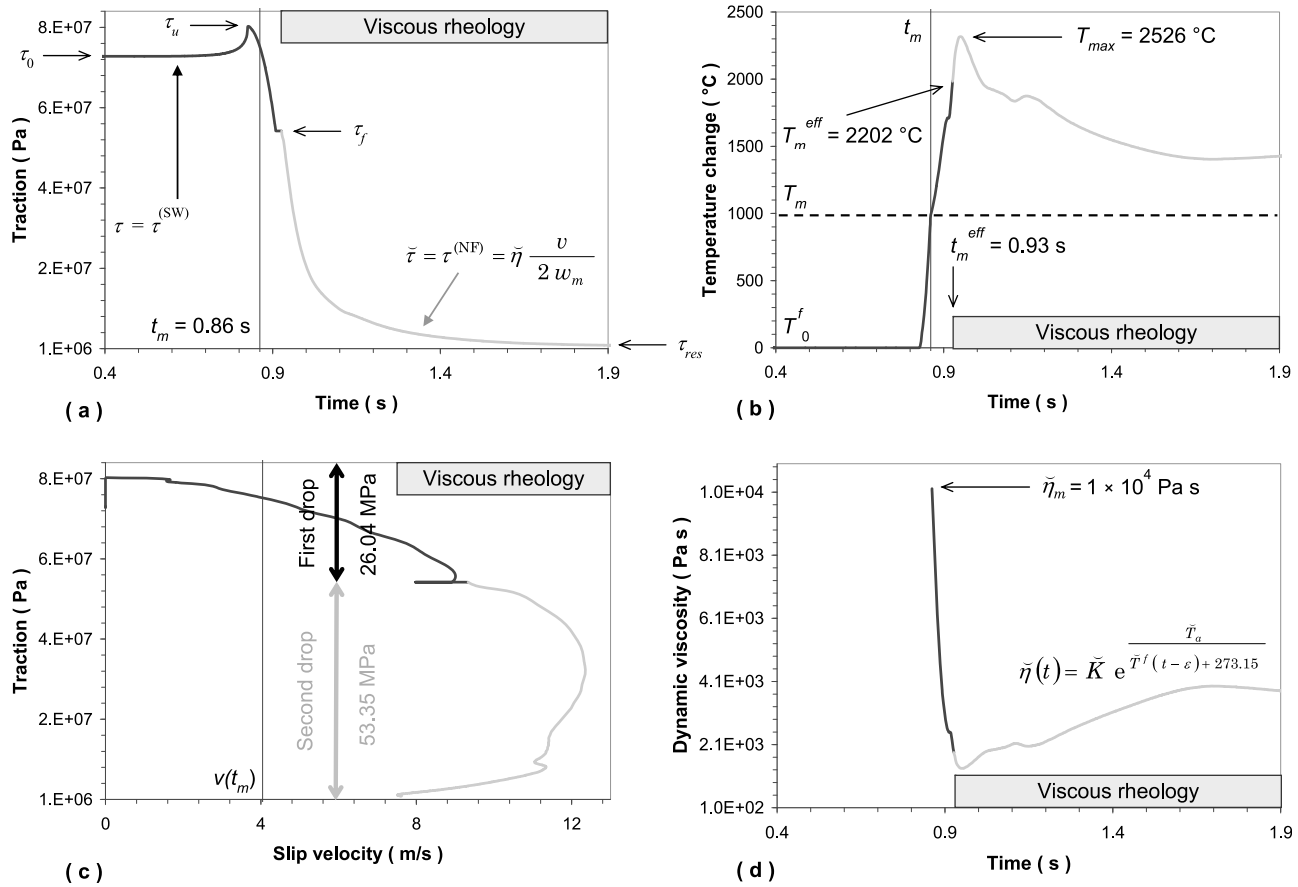

Figure 4. Solutions corresponding to Figures 3b and 3d in a fault point located at the hypocentral depth and at a distance of 3 km from H. (a) Time evolution of frictional resistance. (b) Evolution of temperature change (referred to T_0^f and calculated through equation (24)). (c) Phase portrait (i.e., traction versus slip velocity). (d) Evolution of the dynamic viscosity (see equation (18)). In all plots, the gray portions of the curves (after $t_m^{eff} = 0.93$ s) emphasize when the fault is governed by a viscous rheology (conversely, black portions indicate where SW friction law is paramount).

takes over (t_m^{eff}) and correspondently the value of T_m^{eff} and the critical melt layer half thickness w_{m_c}.

6. The Stefan Problem

[28] In sections 4 and 5, $w_m(t)$ appears as an unknown quantity, but it is necessary to evaluate the fault temperature (equation (24)) and fault traction (equations (21) or (22)). As mentioned above, $w_m(t)$ is determined by considering the Stefan problem, which reads

$$\begin{cases} \dfrac{\mathrm{d}}{\mathrm{d}t} w_m(t) = \dfrac{1}{\rho L}\left(c\chi \dfrac{\partial}{\partial \zeta}\hat{T}(\zeta,t)\Big|_{\zeta=w_m^+(t)} - \breve{c}\breve{\chi}\dfrac{\partial}{\partial \zeta}\breve{T}(\zeta,t)\Big|_{\zeta=w_m^-(t)} \right), \\ w_m(t) = 0 \quad ,\forall\, t \le t_m \end{cases} \tag{25}$$

in which $t \ge t_m$ and L is the latent heat of fusion. Equation (25) expresses the balance between the heat dQ required to change state (i.e., to melt) of a rock mass dm within the

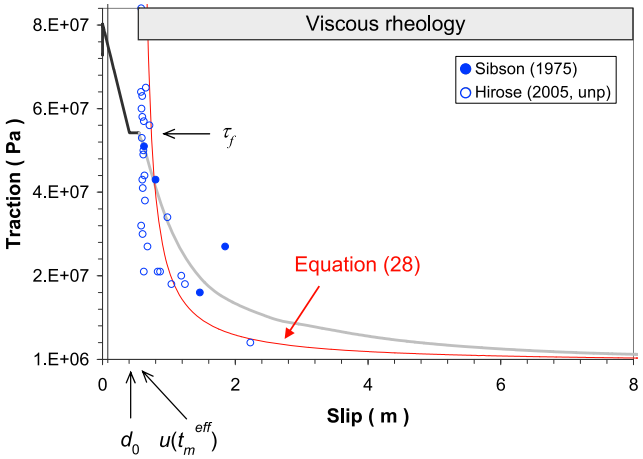

Figure 5. Slip-weakening curve corresponding to the solution reported in Figure 4. Circles represent data field observations from thrusts faults in Outer Hebrides, Scotland (see text for details). Red curve is the estimate of the fault traction as given by equation (28).

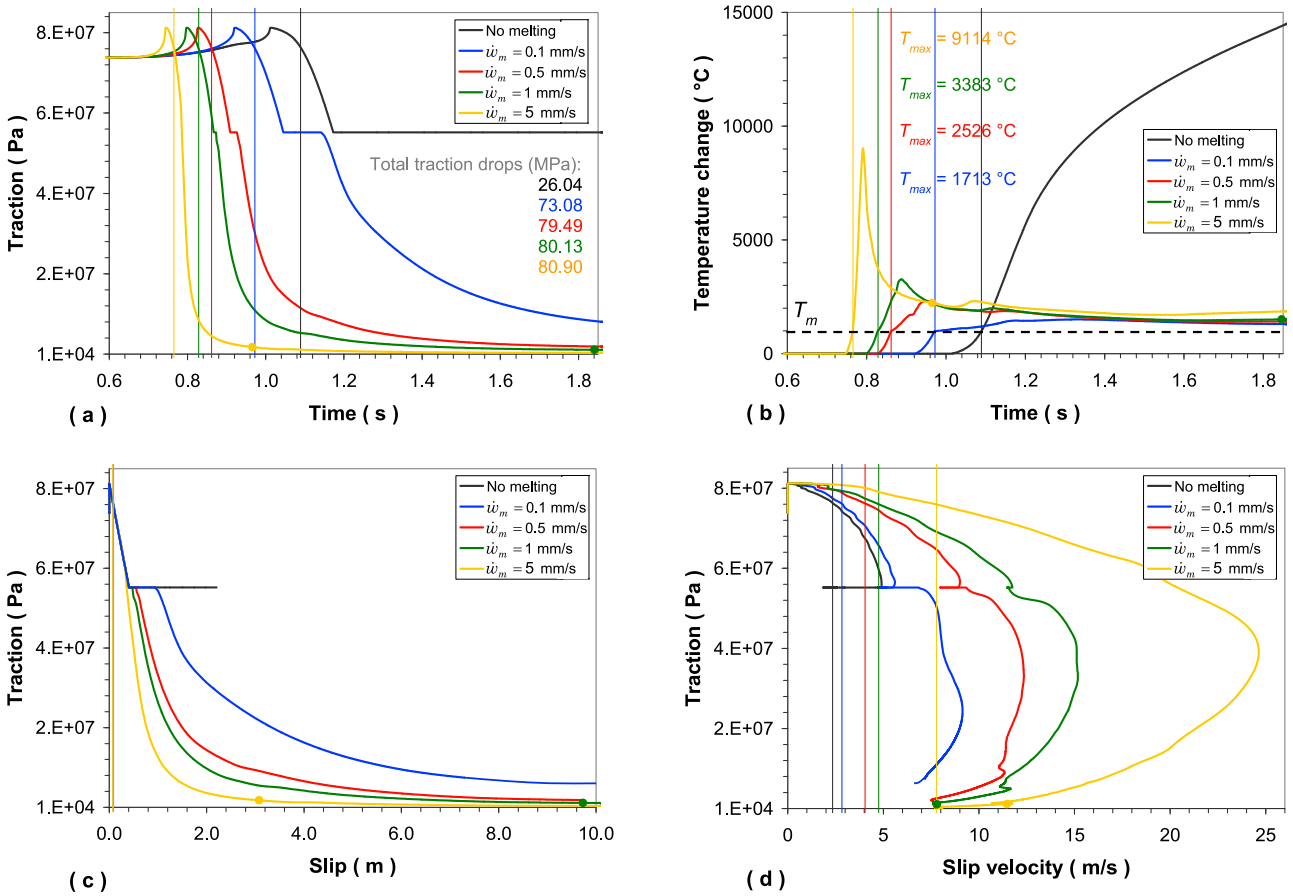

Figure 6. Effects of different time evolutions of the melt layer thickness in the case of a slipping zone 2 mm thick. The w_m follows equation (27), and the different values of $\dot{w}_m$ are reported in the legends (the other parameters are those of Table 1). (a) Time evolution of traction. (b) Time evolution of temperature change. (c) Slip-weakening curve. (d) Phase portrait. Vertical lines indicate when melting locally starts (t_m); big colored circles eventually denote the point where the $w_m = w$ (end limit of our simulations). Black curves pertain to the reference simulation, where melting effects are not considered.

time dt (d$Q = L$ d$m = \rho L$ d$V = \rho L$ dξ_1dξ_3dw_m) and the Fourier heat flux through the melt-solid boundary $\zeta = w_m(t)$

$$q_\zeta^+ - \breve{q}_\zeta^- = c\chi\frac{\partial}{\partial\zeta}\hat{T}(\zeta,t)\Big|_{\zeta=w_m^+(t)} - \breve{c}\,\breve{\chi}\frac{\partial}{\partial\zeta}\breve{T}(\zeta,t)\Big|_{\zeta=w_m^-(t)};$$

all the absorbed energy goes into the phase change (from solid to liquid), without affecting the temperature in the surroundings. The second term on the right-hand side of equation (25) can be obtained from equation (14), which we recall is the solution of the approximation (7) of equation (6). Note also that equation (14) would also require a physical model to describe $\breve{\tau}$ for all ζ and not only on the fault plane; this model requires observational constraints that are presently missed and further investigations. On the other hand, the first term on the right-hand side of equation (25) cannot be calculated from equation (3), since that solution holds only in the phase prior to melting; on the contrary, for $\zeta > w_m(t)$, it can be obtained by solving the following diffusion problem:

$$\begin{cases} \dfrac{\partial}{\partial t}\hat{T}(\xi,t) = \chi\dfrac{\partial^2}{\partial\xi^2}\hat{T}(\xi,t) + \dfrac{\mathrm{d}}{\mathrm{d}t}w_m(t)\dfrac{\partial}{\partial\xi}\hat{T}(\xi,t) + \dfrac{1}{c}\hat{q}(\xi,t) \\ \hat{T}(0,t) = T_m \qquad\qquad ,\forall\, t \geq t_m \end{cases}. \tag{26}$$

In equation (26) the spatial coordinate ξ quantifies the distance from the moving melt-solid boundary and is related to ζ used above through the relation $\xi \equiv \zeta - w_m(t)$ (see Figure 1) and $\hat{q}$ indicate possible additional heat sources or sinks. Similar equations in $\xi' \equiv -\zeta - w_m(t)$ give $\hat{T}$ for $\zeta < -w_m(t)$. (The use of symbol $\hat{T}$ in equations (25) and (26) emphasizes that the temperature is not the same as in equation (3), because we are now dealing with a two-phase problem.)

[29] The problem in equation (26) can be treated analytically by using the Laplace transform, which gives a subsidiary second-order ODE in ξ for the Laplace-transformed function $\tilde{\hat{T}}(\xi;\omega)$, which depends on the temporal frequency

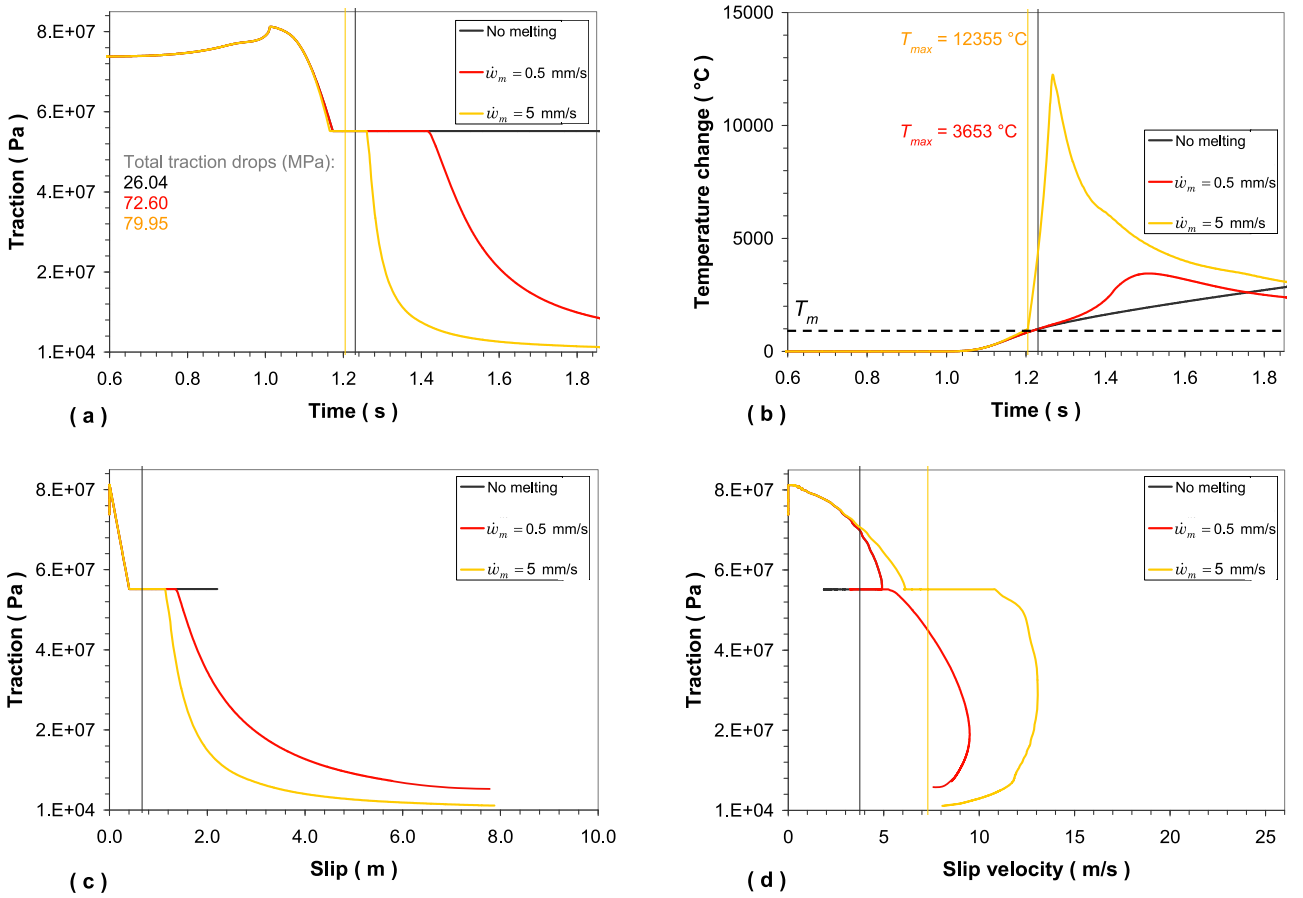

Figure 7. (a-d) The same as in Figure 6 but now with w = 7 mm.

ω. Even in the absence of heat sources or sinks ($\hat{q}$ = 0) the function $\hat{T}(\xi; \omega)$ does not admit a closed-form inverse Laplace transform, so that the analytical solution for $\hat{T}(\xi; t)$ (and for $\hat{T}(\zeta; t)$) remains implicit. As a consequence, the problem in equation (26) has to be solved numerically; this would be the matter of a future study.

7. Numerical Results

[30] It is reasonable that the solution $w_m(t)$ of equation (25) is a sufficiently regular, real function. We can then expand it in a Taylor series in t with initial point in t_m as follows:

$$w_m(t) = w_m(t_m) + \frac{\mathrm{d}}{\mathrm{d}t} w_m \Big|_{t=t_m} (t - t_m) + \frac{1}{2} \frac{\mathrm{d}^2}{\mathrm{d}t^2} w_m \Big|_{t=t_m} (t - t_m)^2 + \ldots .$$

In the remainder of the paper we will consider the first-order approximation of $w_m(t)$; taking into account the condition (12) we have, for $t \geq t_m$,

$$w_m(t) \cong \dot{w}_m (t - t_m), \tag{27}$$

where

$$\dot{w}_m \equiv \frac{\mathrm{d}}{\mathrm{d}t} w_m \Big|_{t=t_m}.$$

We will consider different configurations, by attributing to $\dot{w}_m$ values suggested by observations. We emphasize that this is not the exact solution of the problem in equation (25) coupled with equation (26), but it is its first-order approximation. The conservative assumption that the melt layer enlarges at a constant rate makes the problem tractable analytically and can help us in quantifying the prominent effects of the molten material on the dynamics of a fault. Equation (27) can be thus regarded as a proxy of the true enlarging behavior of the melt layer.

[31] The fully dynamic, spontaneous rupture problem is solved via the finite difference code described by *Bizzarri and Cocco* [2005]. To minimize the spurious numerical reflections originating from the domain boundaries we apply the absorbing boundary conditions described by *Bizzarri and Spudich* [2008]. The rupture nucleates in the imposed hypocenter H (see Figure 2), located at a depth x_3^H = 7 km, and propagates at early states at a constant rupture speed (2.4 km/s [see *Bizzarri*, 2010b]) and then in a fully spontaneous fashion; the fault slips forever, until unbreakable barriers (located the bottom and left ends of the fault) are reached. The adopted parameters are reported in Table 1.

[32] In Figure 3 we report a synoptic comparison between a numerical simulation obeying the linear SW law (equation (16)) over the whole time window considered (Figures 3a and 3c) and another simulation where the effects of melting are accounted for (Figures 3b and 3d). Owing to the

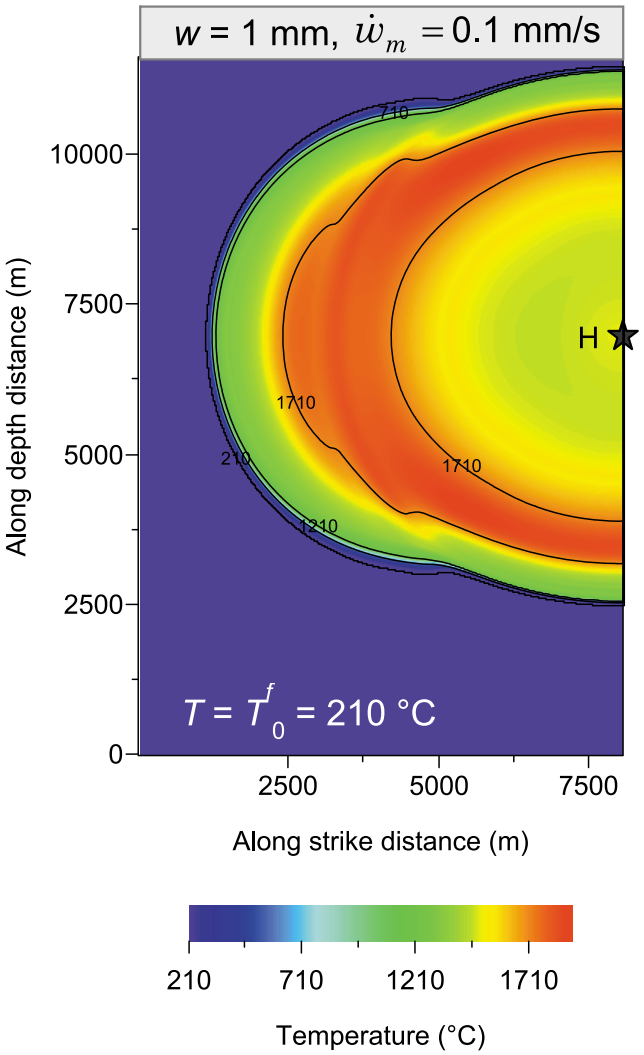

Figure 8. Distribution of temperature on the fault plane a $t = 1.68$ s for a slipping zone 2 mm thick and a melting zone growth rate of 0.1 mm/s (this corresponds to yellow curves in Figure 6).

symmetry exploitation along the strike direction [*Bizzarri*, 2009], we plot only the one half of the fault. When melting is included into the model, we consider $\dot{w}_m = 0.5$ mm/s in equation (27) (a value also suggested by laboratory observations of *Nielsen et al.* [2008, 2010]) and the temperature is calculated from equation (24). The adopted frictional parameters guarantee that the rupture becomes supershear (Figure 3a). However, when a viscous rheology is considered the transition to supershear regime occurs earlier and there are larger patches on the fault with $v_r > v_S$ (Figure 3b; v_r is the rupture speed and v_S is the S waves speed). This indicates that the transition to a viscous rheology as that assumed here enhances the fault instability and therefore promotes the supersonic regime. Correspondently, peaks attained by the fault slip velocity are larger in the case of viscous rheology (compare Figures 3c and 3d). Moreover, the value of the seismic moment at the end of the numerical experiments is rather different; $M_0 = 3.01 \times 10^{18}$ Nm ($M_w = 6.3$) in the reference (i.e., Coulombian) case, while $M_0 = 1.66 \times 10^{19}$ Nm ($M_w = 6.8$) in the viscous case.

[33] Figure 4 shows the solutions for the simulation reported in Figures 3b and 3d in a target fault node. In that location the melting point is reached at $t = t_m = 0.86$ s; after t_m, w_m evolves accordingly to equation (27) and $\breve{\eta}$ follows equation (18). The fault experiences a first traction drop, which namely is the breakdown stress drop, $\Delta\tau_b = \tau_u - \tau_f = 26.04$ MPa. The traction remains at τ_f for a while and then, at $t = t_m^{eff} = 0.93$ s (see equation (23)), the time evolutions of temperature, fault slip velocity, dynamic viscosity and melt layer thickness are such that the viscous shear is dominant with respect to the SW law (equation (16)). According to section 5.3, after t_m^{eff} the fault traction is described by a linearly viscous rheology (equation (21)), emphasized by labels in Figure 4. Owing to the decrease in $\breve{\eta}$ (caused in turn by the temperature increase after t_m^{eff}, see Figure 4b), the traction exhibits a second drop (Figure 4c), which is roughly twice of $\Delta\tau_b$. The total drop is then roughly equal to 80 MPa, which is compatible with observations (see Figure 10 of *Nielsen et al.* [2010], where the dependence of the traction drop on applied normal load is shown). In this numerical experiment the final value of traction is 1.85 MPa (for a Coulomb rheology this would correspond to a friction coefficient equal to 0.015).

[34] The traction versus slip curve (Figure 5) shows a sufficiently good agreement with field data collected on an exhumed seismic thrust fault zone in Outer Hebrides, Scotland (surveyed in 2005 and having a focal depth roughly equal to 10 km; T. Hirose, unpublished data, 2005) and with measurements from *Sibson* [1975] performed on the same fault zone (open and solid blue circles, respectively). We can roughly estimate the value of viscous shear as [cf. *Di Toro et al.*, 2006]

$$\left\langle \breve{\tau} \right\rangle \cong \frac{2\overline{w}_m E \breve{\rho}}{u - u\left(t_m^{eff}\right)}, \tag{28}$$

where $\overline{w}_m$ is the average value of melt layer thickness

$$(\overline{w}_m = \int_{t_m^{eff}}^{t_{end}} \dot{w}_m(t)\mathrm{d}t,$$

which in the present simulation equals $\dot{w}_m(t_{end} - t_m^{eff})$, t_{end} being the final time of the computation) and E is the energy required to produce 1 kg of melt. From equation (28), by assuming $E = 1.76$ MJ/kg and $\breve{\rho}$ as in Table 1 and considering that $\overline{w}_m = 1$ mm and that $u(t_m^{eff}) = 0.56$ m, we obtain the red curve plotted in Figure 5, which is in general agreement with the gray curve in Figure 5 (which in turn represents the result of our model in the viscous regime).

8. Importance of the Melt Layer Evolution

[35] In this section we will explore the effects of different temporal evolutions of the melt layer thickness $2w_m$, by assuming enlarging rates compatible with observations [*Nielsen et al.*, 2008, Table 4]; w_m still obeys equation (27), with the condition $w_m \leq w$. (Again, we recall here that equation (27) is the first-order approximation of the solution of equations (25) and (26)). We consider two different configurations, having $2w = 2$ mm and $2w = 14$ mm, values

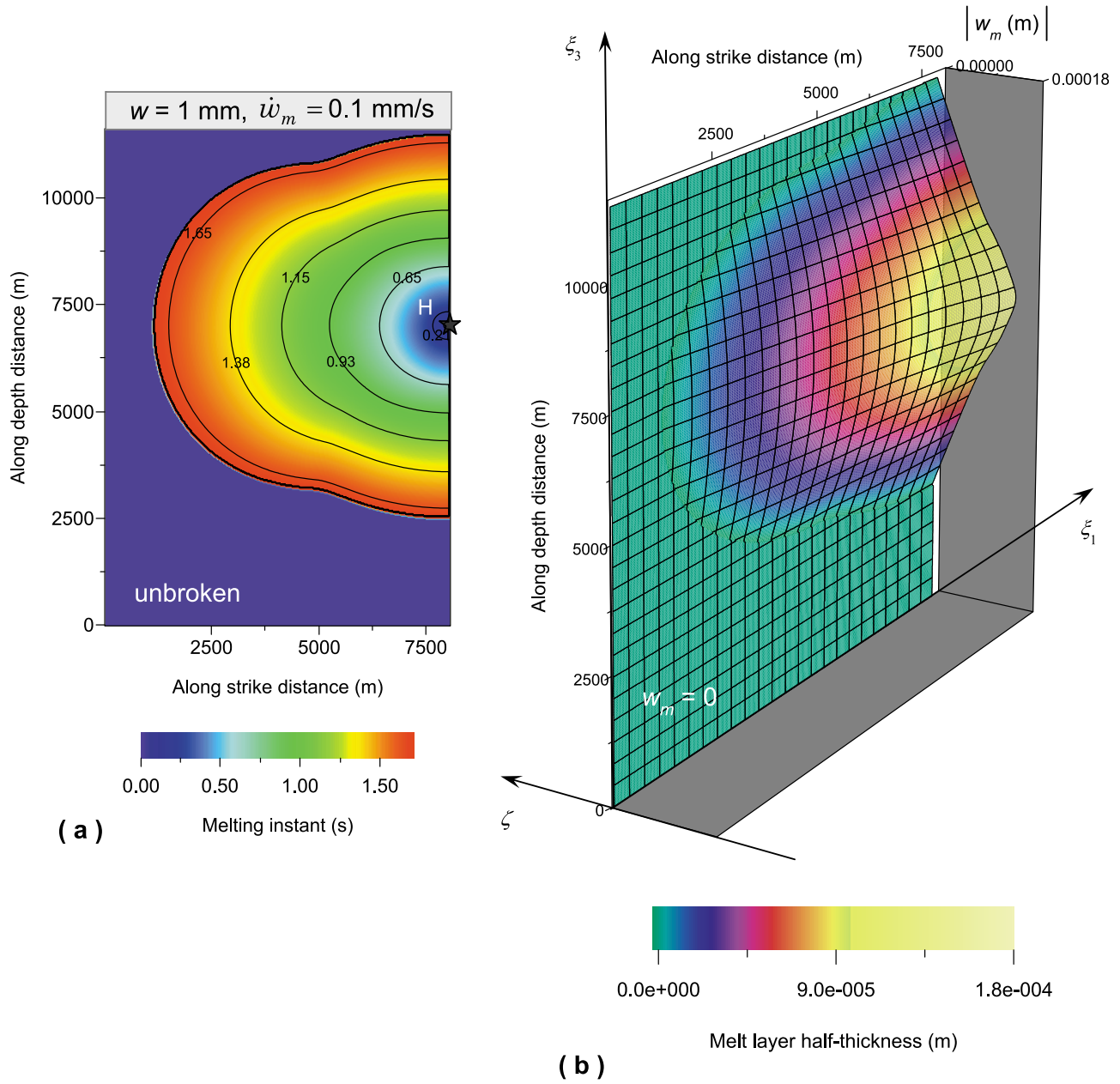

Figure 9. (a) Distribution of melting instant on the fault plane, showing that the minimum is located in the hypocenter H. Purple region denotes the portion of the fault at rest. (b) Corresponding shape of the melt layer half thickness as resulting from equation (27). The referential system $O\xi_1\zeta\xi_3$ of Figure 1 is reported for clarity. Figures 9a and 9b both refer to a numerical simulation where w = 1 mm and $\dot{w}_m$ = 0.1 mm/s.

representative of the slipping zone thickness. The results are reported in Figures 6 and 7, respectively, where we also superimpose the reference solution, that is, the simulation in which melting effects are not considered in the model (black curves in all plots).

[36] It is clear that the time evolution of w_m controls t_m^{eff}, that is, the instant when rheology departs from Coulomb friction and becomes viscous (see section 5.3). In particular, as $\dot{w}_m$ increases the fault remains at the kinetic friction level τ_f for less time (Figures 6a and 7a) and for smaller amount of cumulative slip (Figures 6c and 7c). In the extreme case (w = 1 mm and $\dot{w}_m$ = 5 mm/s; yellow curves in Figure 6) the transition between Coulomb and viscous behavior occurs within the breakdown zone (i.e., for slips smaller than d_0); in this case there are no longer two separate drops in traction, but the fault weakening is continuous.

[37] Correspondingly, the enhanced stress drop at a specific fault point causes a stress redistribution in its surroundings and this increase of dynamic load ultimately causes an increase of rupture speed. This can be clearly seen in Figures 6a and 7a, since the rupture time at the target fault location decreases as $\dot{w}_m$ increases. The same holds for peaks in fault slip velocity; it increases as $\dot{w}_m$ increases (Figures 6d and 7d). Especially in the case of localized shear (w = 1 mm), a faster increasing rate of the melt layer causes a shorter

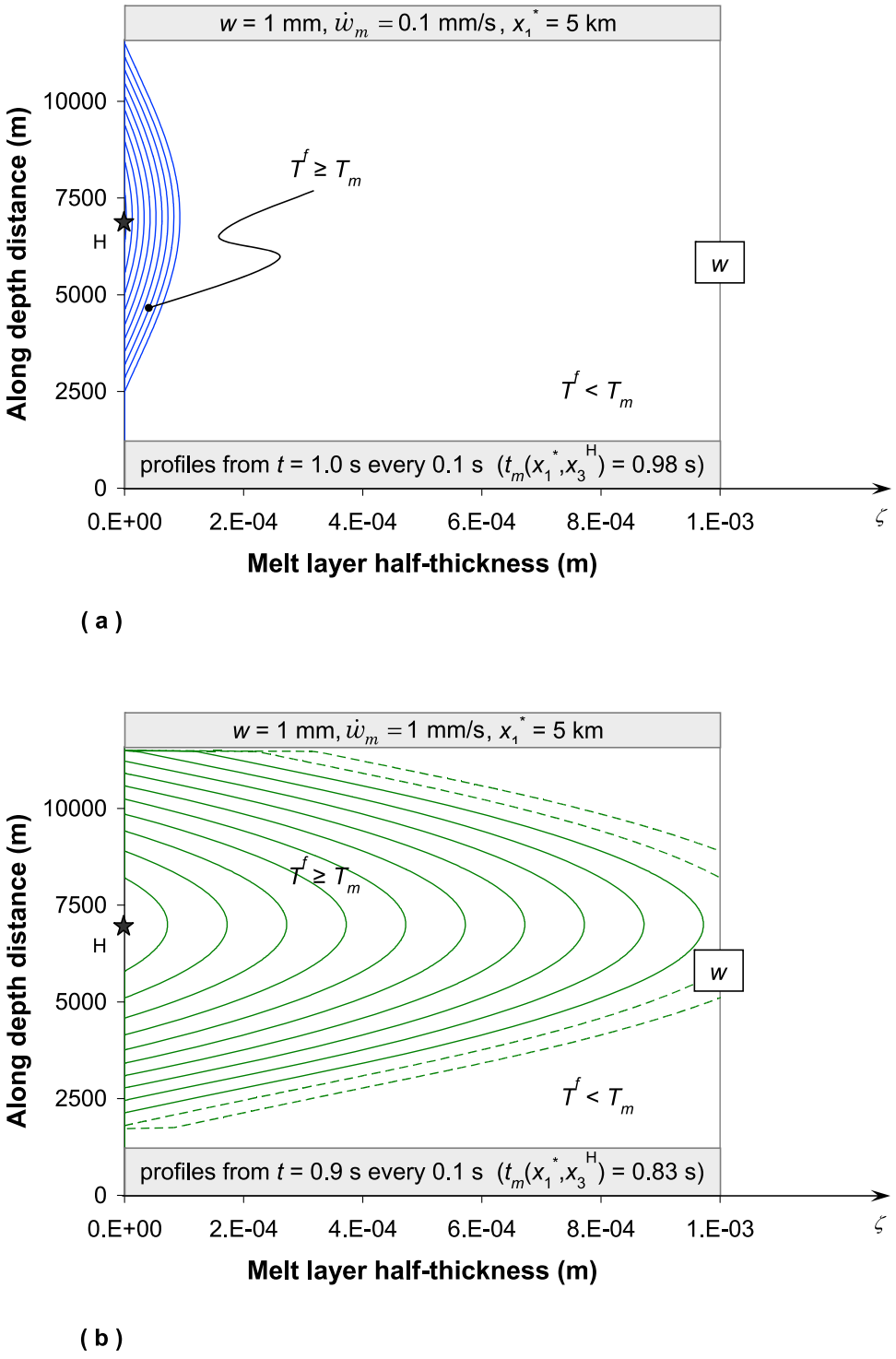

Figure 10. Profiles of w_m as a function of depth calculated at 3 km from the hypocenter along the strike direction (as in Figures 4–7). Each curve is computed every 0.1 s up to the last time level considered in the numerical experiments. Two representative growth rates are assumed: (a) $\dot{w}$ = 0.1 mm/s (as in Figure 9) and (b) $\dot{w}$ = 1 mm/s. In both cases the slipping zone is 2 mm thick. In Figure 10b, dashed curves emphasize when the melt layer thickness exceeds 2w (upper limit in our model; see section 2 for further details). Values of melting instant (as defined by equation (1)) at x_1 = 5 km and $x_3 = x_3^H$ are also indicated.

breakdown zone time (which is the time required for traction to drop from τ_u down to τ_f [*Bizzarri et al.*, 2001]).

[38] With the only exception of $\dot{w}_m$ = 5 mm/s (which is in fact larger than values observed experimentally [see *Nielsen et al.*, 2008]), all models with melting effects develop reasonable temperatures; on the contrary, the case which does not correctly model melting effects (black curves) would produce arbitrarily large temperatures; when w = 1 mm the

temperature predicted by the model at the end of the simulation is larger than the average temperature estimated for the Earth's core. A typical temperature distribution on the mathematical fault plane is reported in Figure 8 for the case of a slipping zone 2 mm wide and for $\dot{w}_m$ = 0.1 mm/s. A fault node of the unbroken region (at rest) remains at T_0^f until rupture front reaches it; then temperature increases, exceeds T_m and then it is controlled by the values of traction and fault slip velocity (see equation (15)).

9. On the Shape of the Melt Layer

[39] The temperature evolution in a fault node depends on the traction and slip velocity histories in that point, as expressed by equation (4). As a consequence, the melting instant t_m would be in fact the two-dimensional array $t_m(x_1, x_3)$. To better quantify this, we plot in Figure 9a the spatial distribution of melting instants in the case of w = 1 mm and $\dot{w}_m$ = 0.1 mm/s. We can clearly see that minimum value of t_m array (which in turn defines the first fault node where melt occurs) is attained at the imposed hypocenter H, which by definition is the first point undergoing to instability. We remark here that for homogeneous rheology and constant and spatially uniform $\dot{w}_m$ the heat production rate is such that the melting temperature is always reached first in H (in other words t_m is minimum in (x_1^H, x_3^H)). The shape of the melt layer half thickness, as given by equation (27), is reported in Figure 9b, from which we can see that w_m is maximum in H (where the term $t - t_m$ is maximum).

[40] In Figure 10 are reported the increasing histories of w_m for two representative values of $\dot{w}_m$. Each line represents the shape of w_m as a function of the depth, calculated at 3 km from the hypocenter (along the strike direction) and every 0.1 s. These profiles confirm that the maximum extension of the melt layer is at hypocentral depths. While for moderate growth rates w_m is quite small with respect to w, when $\dot{w}_m$ is sufficiently high (for instance $\dot{w}_m$ = 1 mm/s as in Figure 10b), it might happen that at the hypocenter w_m exceeds w, which represents the upper limit for our model (as discussed above; see section 2). We emphasize that the shape of the melting layer, during its evolution, depends on the imposed value of $\dot{w}_m$ appearing in equation (27), but it is also controlled by the temperature evolution (which determines $t_m(x_1, x_3)$), which in turn depends on the fault dynamics.

10. Discussion and Conclusions

[41] In this paper we have presented a physical model to account for rocks melting during coseismic earthquake ruptures spontaneously spreading on a fault of finite width, by considering Coulomb friction and viscous rheology in one framework. We have solved the equations of heat transfer in presence of melting, and we have incorporated such a solution in a numerical code to solve the elastodynamic problem. Our solution is in agreement and generalizes previous studies where a constant heat input was considered [*Fialko and Khazan*, 2005; *Nielsen et al.*, 2008, 2010].

[42] In our model we have made some assumptions, briefly recalled here.

[43] 1. We require that the melt layer can reach, at maximum, the boundary of the slipping zone thickness, but it cannot affect the surrounding damage zone (see Figure 1). This assumption is reasonable, since field data reported by *Nielsen et al.* [2010] indicate that the thicknesses of melt layer typically are of the order of a fraction of millimeter, with a few exception reaching several millimeters.

[44] 2. We neglect extrusion dynamics; that is, we do not consider the formation of the injection veins [*Sibson*, 1975]. At the present state of knowledge we do not have sufficient information to analytically model the extrusion process in natural faults, if any [*Sirono et al.*, 2006].

[45] 3. Owing to the small temporal scale pertaining to the breakdown process, during which the stress release takes place, we can safely assume that the temperature inside the melt layer remains well above the melting temperature, T_m, so we can neglect the melt solidification process. This would become potentially important in the postseismic phase of the dynamic rupture, not considered here.

[46] 4. We have also neglected the phenomenon premelting (or surface melting), describing the fact that a quasi-liquid layer (which is in turn temperature-dependent) can appear on crystalline surfaces, even below the T_m.

[47] 5. Most earthquakes happen along faults that contain a range of mineral compositions; for simplicity we have considered here a single value of T_m, which has to be regarded as an average, representative quantification of the melting temperature of the material assemblage in the slipping zone. This is reasonable, in that the boundary between solid and melt appears quite well defined in most laboratory samples and samples from natural faults.

[48] 6. The fault initially obeys the linear SW law and then is governed by a viscous rheology. The transition between a Coulomb rheology to a viscous rheology occurs spontaneously, as discussed in section 5.3, and depends on the evolution of the temperature on the fault surface. We emphasize that the model proposed here can be generalized to other more elaborated Coulombian governing models, such as nonlinear SW equations or rate- and state-dependent friction laws (see *Bizzarri* [2010a] for a review). The adoption of a linear SW friction before melting makes simple the identification of the transition to viscous rheology.

[49] 7. We assume an analytical time evolution of the melt layer thickness $w_m(t)$; it is a first-order approximation of the true behavior of the growing melt layer, which can be obtained only numerically by solving the coupled equations (25) and (26).

[50] Given all the above mentioned limitations of the present model we are able to explore the behavior of a dynamically propagating rupture above the melting temperature (T_m). Otherwise we would have been forced to stop the numerical simulation when T_m was reached in a fault node. Previous theoretical studies [*Bizzarri and Cocco*, 2006a, 2006b; *Fialko*, 2004; *Bizzarri*, 2009, and references therein] clearly indicate that T_m can be easily exceeded, independent of the adopted constitutive equation, provided that the shear is sufficiently localized ($w \leq 1$ mm for representative values of the effective normal stress).

[51] A prominent outcome of the present model is that after melting, the fault experiences a second traction drop which can be twice (or more) the breakdown stress drop predicted by the simple linear SW law (see Figures 4b, 6a, and 7a). Correspondingly, the fracture energy density, which is the amount of energy (for unit fault surface) necessary to maintain an ongoing rupture which propagates on a fault [see

Bizzarri, 2010d, and references therein], increases. This is a consequence of the conservative choice we made, that no viscous braking can occur after melting (see section 5.3).

[52] We also found that the supershear regime is promoted by the transition to a viscous rheology and this can have significant effects on the resulting ground motions [*Dunham and Bhat*, 2008; *Bizzarri et al.*, 2010]. We emphasize that all the previous features are preserved in varying the value of the enlarging rate of the melt layer.

[53] We note that the traction during the viscous stage of the rupture predicted by our model exhibits an exponential decay with time, as early postulated by *Lachenbruch* [1980], theoretically derived by *Matsu'ura et al.* [1992], observed in laboratory experiments by *Ohnaka and Yamashita* [1989], and corroborated by the more recent high-velocity experiments by *Sone and Shimamoto* [2009; see also *Bizzarri*, 2010c]. The viscous behavior we model is also in satisfactory agreement (see Figure 5) with field data from an exhumed seismic thrust fault zone [*Sibson*, 1975; T. Hirose, unpublished data, 2005].

[54] The weakening rate in the viscous regime and the duration of the second traction drop are primarily controlled by the time evolution of the melt layer thickness. The latter can be obtained by solving numerically equations (25) and (26), which surpasses the purposes of the present study. In fact, this would require a consistent physical model to fully describe the behavior of $\breve{\tau}$ for all the coordinates ζ and not only in the mathematical fault plane ($\zeta = 0$; see Figure 1), but this needs further observational constraints. Here we have adopted a first-order approximation of the function $w_m(t)$, as in equation (27), which makes the problem tractable analytically and overcomes the previous theoretical problem.

[55] Further development of this work may be the comparison between our theoretical predictions and high-velocity friction experiments, conducted with time-variable slip velocity histories compatible with those obtained in dynamic models and normal loads representative of seismogenic depths. Finally, systematic microstructural analysis of rock samples can potentially illuminate us about the chemical complexity of natural faults.

Appendix A: Properties of the Temperature Inside the Melt Layer

A1. Comparison With Previous Solution

[56] In this appendix we will analyze the temperature evolution within the molten region. As discussed in the main text, the analytical solution for $\breve{T}$ is given by equation (14), which reduces to equation (15) in the center of the melt layer (i.e., on the mathematical fault plane $\zeta = 0$; see Figure 1).

[57] *Nielsen et al.* [2008] (and *Nielsen et al.* [2010] as well) solve the heat conduction equation (6) in a static (i.e., time independent) configuration. Their solution cannot be expressed in a closed form as a function of w_m, so they apply an approximation of boundary condition for the flux at the melt-solid boundary:

$$\left.\frac{\partial}{\partial\zeta}\breve{T}\right|_{\zeta=w_m^-} \cong -\frac{\tau_a v_a}{2\,\breve{c}\breve{\chi}}, \tag{A1}$$

where τ_a is the constant applied stress and v_a is the applied sliding velocity (see equation (16) of *Nielsen et al.* [2008]; note also that in our notation, $\breve{c}$ is equivalent to $\breve{\rho}\breve{c}$ in the notation of *Nielsen et al.* [2008]). Correcting a misprint in their equation (B2), they obtain

$$\overset{\smile}{T}^{NEA}(\zeta) = T_m - T_c \log\left(\frac{\cosh^2\left(\dfrac{2\zeta\tau_a}{\breve{\eta}_c W}\sqrt{\dfrac{v_a^2}{W^2}+1}\right)}{\dfrac{v_a^2}{W^2}+1}\right) \tag{A2}$$

(see also equations (34) and (35) of *Nielsen et al.* [2008]). Simple algebra shows that the function $\breve{T}^{NEA}(\zeta)$ does not satisfy the boundary condition $\breve{T}^{NEA}(\pm w_m) = T_m$ for arbitrary values of melt layer half thickness, but only if w_m equals a specific value, w_m^*:

$$w_m^* = \frac{W\breve{\eta}_m}{2\tau_a}\frac{\operatorname{atgh}\left(\dfrac{v_a}{W\sqrt{\frac{v_a^2}{W^2}+1}}\right)}{\sqrt{\dfrac{v_a^2}{W^2}+1}}. \tag{A3}$$

[58] Let we now consider our solution for $\breve{T}^f(\zeta, t)$ (see equation (14)) and let us consider the temporal averages (for times $t \geq t_m$) of time variable quantities appearing therein; we can write

$$\overline{\breve{T}}(\zeta) = T_m - \left[\frac{\zeta\,\mathrm{erf}\left(\dfrac{\zeta}{\sqrt{2}\overline{w}_m}\right)}{2\,\breve{c}\breve{\chi}} - \frac{\left(\sqrt{\dfrac{2\pi}{\mathrm{e}}} + \pi\,\mathrm{erf}\left(\dfrac{1}{\sqrt{2}}\right) - \sqrt{2\pi}\mathrm{e}^{-\frac{\zeta^2}{2\overline{w}_m^2}}\right)\overline{w}_m}{2\pi\,\breve{c}\breve{\chi}}\right]\overline{\breve{\tau}}\,\overline{\breve{v}}. \tag{A4}$$

[59] If we associate the quantities $\overline{\breve{\tau}} \leftrightarrow \tau_a$ and $\overline{\breve{v}} \leftrightarrow v_a$, we can directly compare the temperature distribution as a function of the distance from the center of the melt layer obtained here (equation (14), or its time average, equation (A4)) with the solution of *Nielsen et al.* [2010] (see equation (A2)).

[60] On the other hand, *Fialko and Khazan* [2005, equation (22)], in the isoviscous approximation independently found another expression for $\breve{T}^f(\zeta, t)$:

$$\overset{\smile}{T}^{FK}(\zeta) = T_m + \frac{v_a^2\breve{\eta}_m}{2\,\breve{c}\breve{\chi}}\left(1 - \frac{\zeta^2}{w_m^2}\right). \tag{A5}$$

The result of the comparison between the three different equations (equation (14), or its time average in equation (A4); (A2); and (A5)) is reported in Figure A1. We select three representative values of the sliding speed, $v_a = 0.1$ m/s (Figure A1a), $v_a = 1$ m/s (Figure A1b) and $v_a = 10$ m/s (Figure A1c). Note that to make possible the comparison we use in (A4) $\overline{w}_m = w_m^*$ as given by equation (A3), since it is the only value which satisfies condition (9) for the solution of *Nielsen et al.* [2008, 2010]. Analogously, in equation (A5) we also use $w_m = w_m^*$.

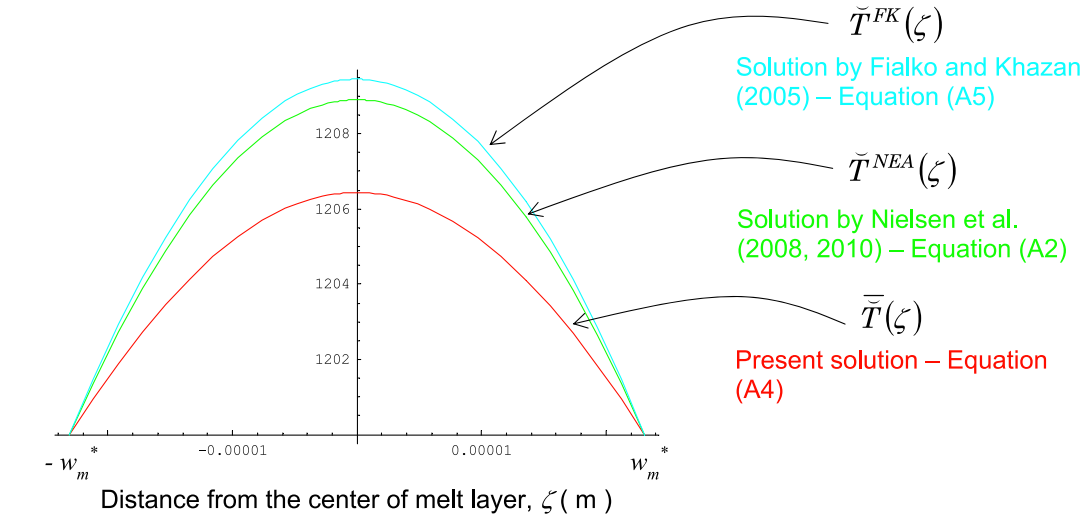

(a)

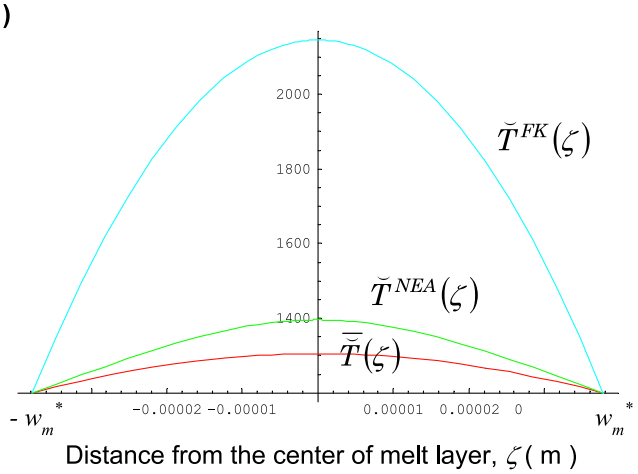

(b)

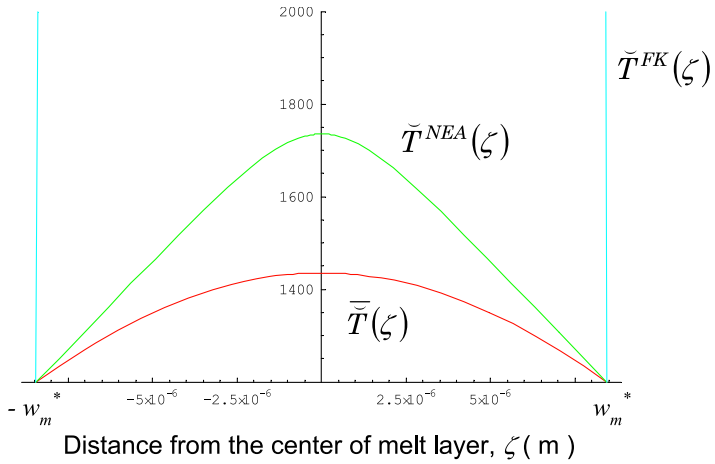

(c)

Figure A1. Comparison between the solution obtained by *Nielsen et al.* [2008, 2010], $\breve{T}^{NEA}(\zeta)$ (see equation (A2)), that from *Fialko and Khazan* [2005], $\breve{T}^{NEA}(\zeta)$ (equation (B5)), and the time-averaged solution obtained in the present paper, $\overline{\breve{\tau}}(\zeta)$ (see equation (A4)). For the comparison, we use $\overline{\breve{\tau}} = \tau_a =$ 20 MPa and $\overline{w}_m = w_m^*$ as given by equation (A3); the other constitutive parameters are tabulated in Table 1. Values in ordinate axis are in degrees Celsius. (a) $\overline{v} = v_a = 0.1$ m/s. (b) $\overline{v} = v_a = 1$ m/s. (c) $\overline{v} = v_a = 10$ m/s. The resulting values of w_m^* are 23.1, 37.8, and 8.45 μm, respectively.

[61] We can clearly see that in all three models the maximum temperature is realized in the center of the melt zone (as physically expected) and it gradually decreases near the melt-solid boundaries. For decreasing melt layer thickness the temperature values are higher, as they should be, and the curves become more peaked at $\zeta = 0$. The maximum values of temperature predicted by the present model are smaller that those predicted by the model of *Nielsen et al.* [2008, 2010] and by *Fialko and Khazan* [2005]. The latter gives wrong predictions for high speeds (see Figure A1c). On the contrary, for moderate speed all the three models are quite comparable (see Figure A1a).

[62] We emphasize that this comparison assumes the time averages of the time variable quantities w_m, $\breve{\tau}$ and v over the temporal window of interest appearing in equation (14), so that comparison is indicative of a general behavior.

A2. Time Evolution in the Center of the Melt Layer

[63] Let us now consider the solution for the temperature evolution in the center of the melt layer. From equation (15) we have that the prefactor

$$C \equiv \left(\sqrt{\frac{2\pi}{\mathrm{e}}} + \pi \,\mathrm{erf}\left(\frac{1}{\sqrt{2}}\right) - \sqrt{2\pi} \right)$$

is nearly equal to 1.16. By considering that w_m, $\breve{\tau}$ and v are all positive quantities by definition, we have that T^f can assume values greater than T_m, or, in other words, that we can have the superheating phenomenon. This feature has been also found in laboratory experiments by *Nielsen et al.* [2010], and it also confirmed by results reported in Figure A1.

A3. Boundary Condition at $\zeta = \bar{w}_m(t)$

[64] The Stefan problem (see equation (25)) relates the spatial derivatives of solid and melt temperature calculated at the melt-solid boundaries ($\zeta = \pm w_m(t)$) to the growth rate of the melt layer $\dot{w}(t)$. *Nielsen et al.* [2008] found an approximate relation expressing heat flux $\breve{q}_{\bar{\zeta}}$ leading to equation (A1) previously reported.

[65] From equation (14), by considering the time averages, we have

$$\left.\frac{\partial}{\partial\zeta}\breve{T}(\zeta,t)\right|_{\zeta=w_m^{-}(t)} \cong -\frac{1}{2\,\breve{c}\,\breve{\chi}}\,\mathrm{erf}\left(\frac{1}{\sqrt{2}}\right)\bar{\breve{\tau}}\bar{v}, \tag{A6}$$

which in agreement with equation (A1), taking into account that $\mathrm{erf}(1/\sqrt{2}) = 0.7$.

Appendix B: A Posteriori Verification That $\partial\breve{T}/\partial t$ Term in Equation (6) Can Be Neglected

[66] Equation (7) assumes that

$$\left|\frac{\partial\breve{T}}{\partial t}\right| \ll \left|\frac{\breve{q}}{\breve{c}}\right|.$$

By assuming $\breve{q}$ as in equation (13) we obtain the solution (14) (or solution (15) in the center of the melt layer $\zeta = 0$; see Figure 1). Let us assume that t is such that $\breve{\tau} = \tau^{(\mathrm{NF})}$ (see sections 5.2 and 5.3 for further details on fault rheology in the melting regime). The temperature (and its temporal variation) is maximum for $\zeta = 0$. Therefore, by considering equations (17) and (19), from equation (15) we have

$$\left|\frac{\partial\breve{T}^f(t)}{\partial t}\right| = \frac{\breve{\eta}\,C}{2\pi\,\breve{c}\,\breve{\chi}}\,v(t)\left|\frac{\partial v}{\partial t}\right| \tag{B1}$$

with C defined above. On the other hand, we also have that $\breve{q}/\breve{c}$ is maximum for $\zeta = 0$; from equation (13) we have

$$\left|\frac{\breve{q}}{\breve{c}}\right| = \frac{\breve{\eta}}{\sqrt{2\pi}\,\breve{c}\,w_m(t)}\,v^2(t). \tag{B2}$$

[67] In conclusion, equation (15) is a valid solution of equation (6) if the following condition is satisfied:

$$\frac{1}{v(t)}\left|\frac{\partial v(t)}{\partial t}\right| \ll \frac{\sqrt{2\pi}\,\breve{\chi}}{C}\,\frac{1}{w_m^2(t)} \tag{B3}$$

for all arbitrary times t such that such that $\breve{\tau} = \tau^{(\mathrm{NF})}$. Interestingly, condition (B3) is independent of the dynamic viscosity; it only relates melt layer half thickness for fault slip velocity and fault slip acceleration. Equation (B3) may also be physically interpreted as a condition on the melt layer thickness; until $w_m(t)$ is such that

$$w_m^2(t) \ll \frac{\sqrt{2\pi}\,\breve{\chi}}{C}\,\frac{v(t)}{\left|\frac{\partial v(t)}{\partial t}\right|}, \tag{B4}$$

the equation (15) is a valid solution of equation (6). On the contrary, when condition (B4) is violated, the analytical solution in equation (15) is no longer valid, and therefore equation (6) can be solved only numerically.

[68] We also conclude emphasizing that the condition

$$\left|\frac{\partial\breve{T}}{\partial t}\right| \ll \left|\frac{\breve{q}}{\breve{c}}\right|$$

does not conflict with the time variability of $\breve{T}$, explicitly stated in equations (14) and (15) and obtained in our numerical experiments.

[69] The numerical experiments presented and discussed in the present paper satisfy both condition (B3) and condition (B4).

Appendix C: Validity of Equation (18) for Dynamic Viscosity Evolution

[70] The Arrhenius equation applied to dynamic viscosity of a melt material [see *Shaw*, 1972; *Dingwell*, 1998] postulates a dependence on the absolute temperature, which reads

$$\breve{\eta} = \breve{K}\,\mathrm{e}^{\frac{\breve{T}_a}{\breve{T}}}, \tag{C1}$$

where $\breve{K}$ is a constant preexponential factor and $\breve{T}_a$ is the activation temperature. Equation (18) follows from equation (C1) simply by putting the absolute temperature

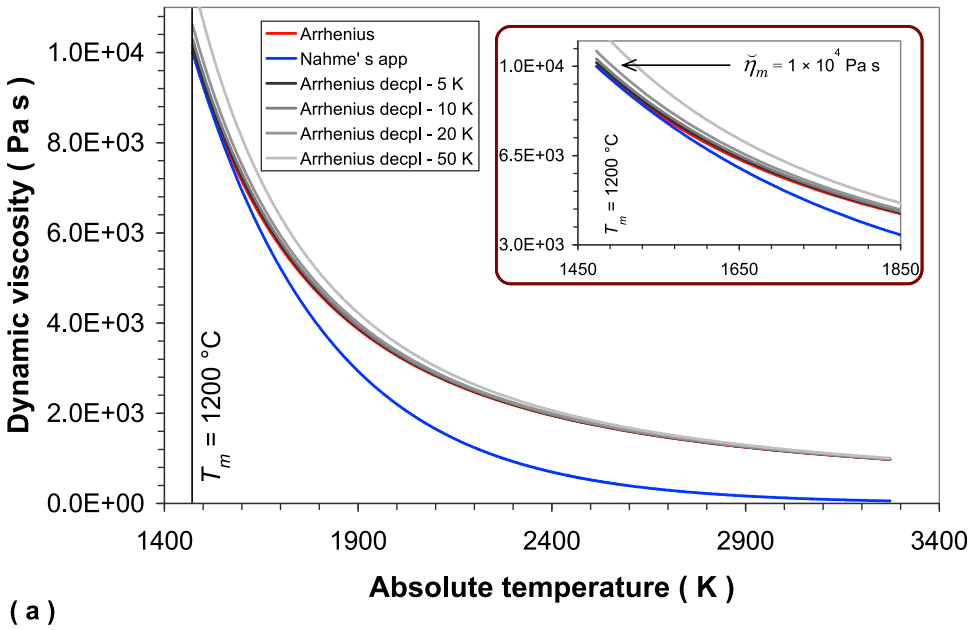

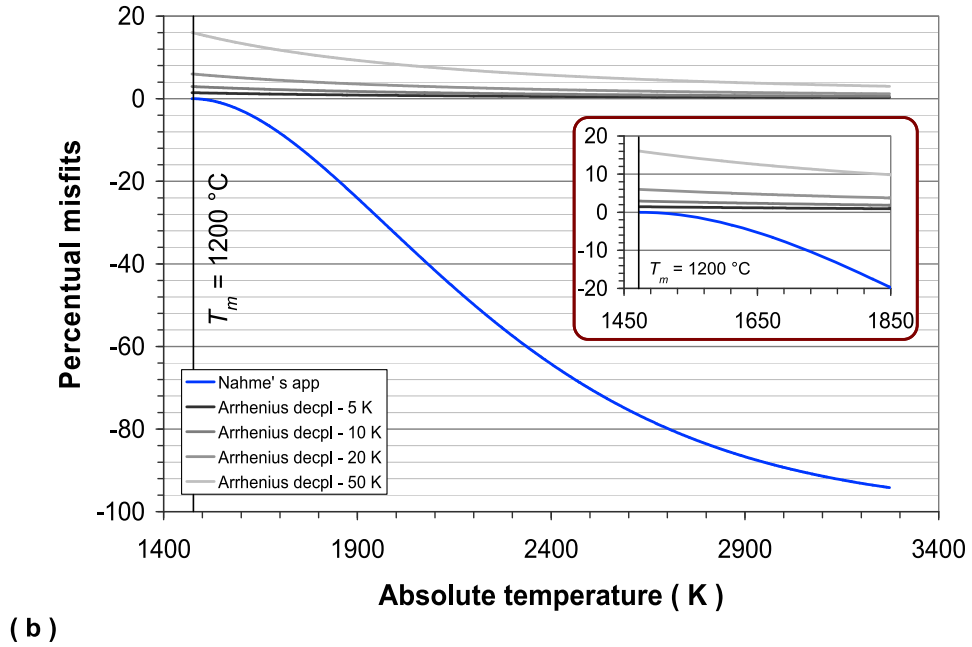

Figure C1. (a) Comparison between different evolution laws for dynamic viscosity of the melt material for a typical temperature interval above the melting point. Red curve is the original Arrhenius law (equation (C1)). Blue curve is its Nahme's approximation (equation (C2), or equivalently (C3)). Black and gray curves pertain to the approximation adopted in the present paper, in which the temperature entered into the Arrhenius equation is computed at the previous time level (see equation (18)). (b) Normalized differences of the various approximations with respect to the true prediction given by the Arrhenius equation (equation (C1)); in the ordinate axis, for each temperature value, we plot the quantity $100(\breve{\eta}^{(\text{approximation})} - \breve{\eta}^{(\text{Arrhenius})})/\breve{\eta}^{(\text{Arrhenius})}$. In the legends are indicated the different values of the differences of temperature, $\Delta\breve{T}$ at time level, m, and at its subsequent time level, $m + 1$ ($\Delta\breve{T}$ = 5, 10, 20, and 50 K). The adopted parameters are those listed in Table 1.

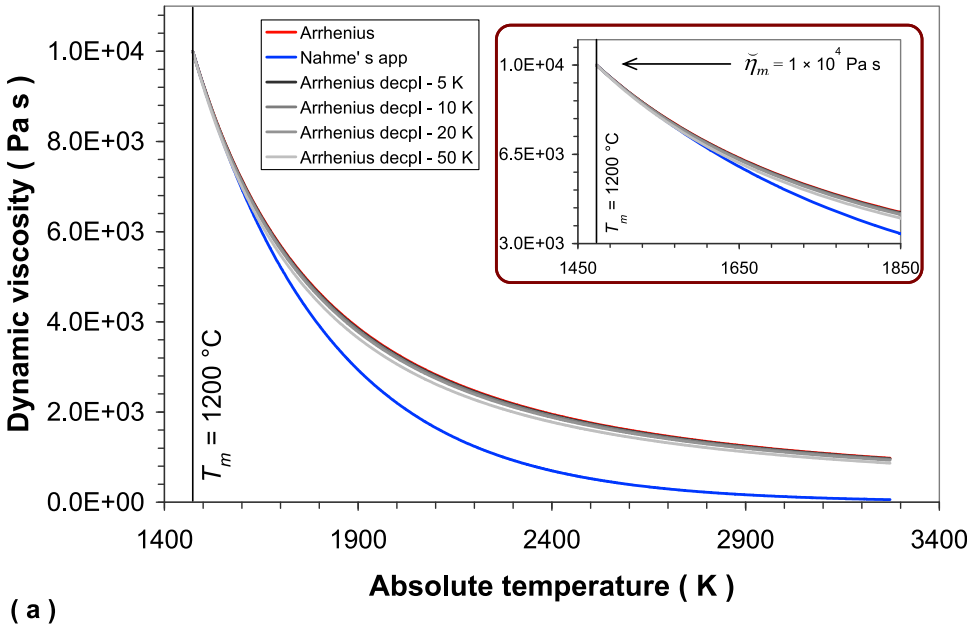

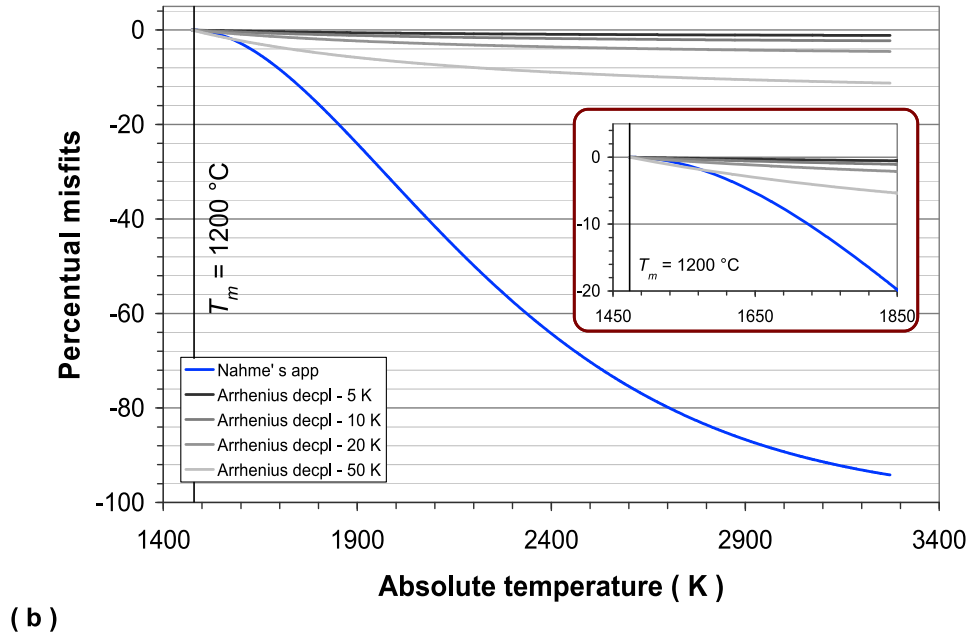

Figure C2. (a and b) The same as in Figure C1, but now black and gray curves refer to our approximation in equation (18) with the preexponential factor as in equation (C4); in such a way, in all cases the dynamic viscosity at melting temperature identically equals $\breve{\eta}_m = 1 \times 10^4$ Pa s. The values of $\breve{K}'$ from equation (C4) are 143.29, 141.23, 137.15, and 125.29 Pa s, for $\Delta\breve{T} = 5$, 10, 20, and 50 K, respectively.

inside the melt layer (so that T in equation (C1) is expressed as $\breve{T} + 273.15$, where $\breve{T}$ is as in equation (14) or equation (15) is in °C). Moreover, in equation (18) we consider the temperature at the previous elastodynamic time step ($t - \varepsilon$ formally is $t^{(m)} - \Delta t$, where $t^{(m)} = m\Delta t$ is the discrete time at level m and Δt is the time step).

[71] In this appendix we will quantitatively evaluate the goodness of such an assumption by considering typical scenarios for temperature evolution. In the synoptic comparison we will also consider the Nahme's approximation of equation (C1), which has been often considered in the literature [*Costa and Macedonio*, 2002; *Nielsen et al.*, 2008, 2010]:

$$\breve{\eta} = \breve{\eta}_m \mathrm{e}^{-\frac{\breve{T}-\breve{T}_m}{\breve{T}_c}}, \tag{C2}$$

where

$$\breve{\eta}_m \equiv \breve{K}\, e^{\breve{T}_a/\breve{T}_m}$$

and $\breve{T}_c \equiv \breve{T}_m^2/\breve{T}_a$. After simple algebra we can rewrite equation (C2) as follows:

$$\breve{\eta} = \breve{K}\, e^{\frac{\breve{T}_a\left(2\breve{T}_m - \breve{T}\right)}{\breve{T}_m^2}}. \tag{C3}$$

By assuming the same parameters as those of *Nielsen et al.* [2008], $\breve{\eta}_m = 1 \times 10^4$ Pa s, $\breve{T}_c = 75°C = 348.15$ K and $\breve{T}_m = 1200°C = 1473.15$ K, we obtain the two parameters of equation (C1) as listed in Table 1 ($\breve{K} = 154.37$ Pa s and $\breve{T}_a = 6233$ K).

[72] In Figure C1 we report the comparison (by adopting the above mentioned values) of the original Arrhenius law (red curve), its Nahme's approximation (blue curve) and the approximation adopted in the present paper, equation (18), as obtained by assuming that the temperature increase from a time level to its subsequent time level is 5, 10, 20 and 50 K (black and gray curves). In other words we assume that $\Delta\breve{T} \equiv \breve{T}(t^{(m)}) - \breve{T}(t^{(m)} - \Delta t) = 5$, 10, 20 and 50 K.

[73] From Figure C1 we can immediately see that the Nahme's approximation is valid only for a small interval after the melting point; this is not surprising, since equation (C2) has been obtained by considering the Taylor expansion of the term $\breve{T}_a/T$ appearing in equation (C1) in the vicinity of $T = T_m$. Nevertheless, Figure C1 clearly demonstrates that for temperatures greater than about 1600°C (which can be easily realized in the center of the melt layer; see Figure 4b of *Nielsen et al.* [2008]), equation (C2) significantly differs from equation (C1), more than the approximation used in the present paper. From Figure C1b we have that at $T = 1600°C$ the Nahme's approximation differs from true value of the Arrhenius equation more than 21% of the Arrhenius value. On the contrary, with the approximation used in the present study (equation (18)), these percentage differences are 0.9%, 1.8%, 3.7% and 9.6% for $\Delta\breve{T} = 5$, 10, 20 and 50 K, respectively. In other words, equation (C2) gives a biased value of dynamic viscosity for temperature roughly greater than T_m + 300°C. On the contrary, we can notice an overall good agreement of the approximation adopted in the present paper ($T = \breve{T}(t^{(m)} - \Delta t) + 273.15$) with respect to the reference case of equation (C1) for a wide range of temperatures.

[74] For temperatures close to T_m the agreement between equations (C1) and (18) remains good (see Figures C1a and C1b), provided that the increments of temperature from one elastodynamic time level and its subsequent are 20 K at maximum. This condition can be easily satisfied by considering a sufficiently fine temporal discretization, as such adopted in the numerical experiments presented in this paper (see Table 1).

[75] The differences between equations (C1) and (18)) for temperatures near the melting point can be easily reduced as follows. Let us consider in equation (18) the preexponential constant to be

$$\breve{K}' \equiv \breve{K}\, e^{-\frac{\breve{T}_a \Delta\breve{T}}{\breve{T}_m\left(\breve{T}_m - \Delta\breve{T}\right)}} \tag{C4}$$

instead of $\breve{K}$. In such a way at the melting temperature T_m all the approximations give exactly the same value of dynamic viscosity, that is, $\breve{\eta}_m = 1 \times 10^4$ Pa s. The replacement of K with $\breve{K}'$ merely represents a shift in the ordinate axis. (In the ideal case of arbitrarily small $\Delta\breve{T}$ we have that $\breve{K}'$ of equation (C4) reduces to $\breve{K}$).

[76] The behavior of $\breve{\eta}$ as predicted by the various approximation for increasing temperatures is reported in Figure C2a; in the present case we use in equation (18), $\breve{K}'$ as in equation (C4). From Figure C2a we can immediately see that the agreement of our approximate relation (equation (18)) and the original Arrhenius equation is now remarkably good over the whole range of considered temperatures (compare the inset plots in Figures C1b and C2b). At large temperatures the agreement remains good; at $T = 1600°C$ the percentage misfits are now −0.6%, −1.1%, −2.2%, and −5.6% for $\Delta\breve{T} = 5$, 10, 20, and 50 K, respectively (see Figure C2b).

[77] **Acknowledgments.** We thank S. Nielsen for providing material in advance of publication. D. Ogelsby, two anonymous referees, the associate editor, and the editor, R. Nowack, are kindly acknowledged for useful comments that helped to improve the manuscript.

References

Andrews, D. J. (2002), A fault constitutive relation accounting for thermal pressurization of pore fluid, *J. Geophys. Res.*, *107*(B12), 2363, doi:10.1029/2002JB001942.

Bizzarri, A. (2009), Can flash heating of asperity contacts prevent melting?, *Geophys. Res. Lett.*, *36*, L11304, doi:10.1029/2009GL037335.

Bizzarri, A. (2010a), Toward the formulation of a realistic fault governing law in dynamic models of earthquake ruptures, in *Dynamic Modelling*, edited by A. V. Brito, pp. 167–188, InTech, Vienna. (Available at http://sciyo.com/articles/show/title/toward-the-formulation-of-a-realistic-fault-governing-law-in-dynamic-models-of-earthquake-ruptures)

Bizzarri, A. (2010b), How to promote earthquake ruptures: Different nucleation strategies in a dynamic model with slip-weakening friction, *Bull. Seismol. Soc. Am.*, *100*(3), 923–940, doi:10.1785/0120090179.

Bizzarri, A. (2010c), An efficient mechanism to avert frictional melts during seismic ruptures, *Earth Planet. Sci. Lett.*, *296*, 144–152, doi:10.1016/j.epsl.2010.05.012.

Bizzarri, A. (2010d), On the relations between fracture energy and physical observables in dynamic earthquake models, *J. Geophys. Res.*, *115*, B10307, doi:10.1029/2009JB007027.

Bizzarri, A. (2010e), On the recurrence of earthquakes: Role of wear in brittle faulting, *Geophys. Res. Lett.*, *37*, L20315, doi:10.1029/2010GL045480.

Bizzarri, A., and M. Cocco (2005), 3D dynamic simulations of spontaneous rupture propagation governed by different constitutive laws with rake rotation allowed, *Ann. Geophys.*, *48*(2), 279–299.

Bizzarri, A., and M. Cocco (2006a), A thermal pressurization model for the spontaneous dynamic rupture propagation on a three-dimensional fault: 1. Methodological approach, *J. Geophys. Res.*, *111*, B05303, doi:10.1029/2005JB003862.

Bizzarri, A., and M. Cocco (2006b), A thermal pressurization model for the spontaneous dynamic rupture propagation on a three-dimensional fault: 2. Traction evolution and dynamic parameters, *J. Geophys. Res.*, *111*, B05304, doi:10.1029/2005JB003864.

Bizzarri, A., and P. Spudich (2008), Effects of supershear rupture speed on the high-frequency content of S waves investigated using spontaneous dynamic rupture models and isochrone theory, *J. Geophys. Res.*, *113*, B05304, doi:10.1029/2007JB005146.

Bizzarri, A., M. Cocco, D. J. Andrews, and E. Boschi (2001), Solving the dynamic rupture problem with different numerical approaches and constitutive laws, *Geophys. J. Int.*, *144*, 656–678, doi:10.1046/j.1365-246x.2001.01363.x.

Bizzarri, A., E. M. Dunham, and P. Spudich (2010), Coherence of Mach fronts during heterogeneous supershear earthquake rupture propagation: Simulations and comparison with observations, *J. Geophys. Res.*, *115*, B08301, doi:10.1029/2009JB006819.

Costa, A., and G. Macedonio (2002), Nonlinear phenomena in fluids with temperature-dependent viscosity: An hysteresis model for magma flow in conduits, *Geophys. Res. Lett.*, *29*(10), 1402, doi:10.1029/2001GL014493.

Dieterich, J. H. (1979), Modelling of rock friction: 1. Experimental results and constitutive equations, *J. Geophys. Res.*, *84*, 2161–2168, doi:10.1029/JB084iB05p02161.

Dingwell, D. (1998), Melt viscosity and diffusion under elevated pressures, *Rev. Mineral.*, *37*, 397–424.

Di Toro, G., T. Hirose, S. Nielsen, and T. Shimamoto (2006), Relating high-velocity rock-friction experiments to cosesimic slip in presence of melts, in *Radiated Energy and the Physics of Earthquake Faulting*, *Geophys. Monogr. Ser.*, vol. 170, edited by R. Abercrombie et al., pp. 121–134, AGU, Washington, D. C.

Dunham, E. M., and H. S. Bhat (2008), Attenuation of radiated ground motion and stresses from three-dimensional supershear ruptures, *J. Geophys. Res.*, *113*, B08319, doi:10.1029/2007JB005182.

Evans, J. P., and M. Chester (1995), Fluid-rock interaction in faults of the San Andreas system: Inferences from San Gabriel fault rock geochemistry and microstructures, *J. Geophys. Res.*, *100*, 13,007–13,020, doi:10.1029/94JB02625.

Fialko, Y. A. (2004), Temperature fields generated by the elastodynamic propagation of shear cracks in the Earth, *J. Geophys. Res.*, *109*, B01303, doi:10.1029/2003JB002497.

Fialko, Y., and Y. Khazan (2005), Fusion by earthquake fault friction: Stick or slip?, *J. Geophys. Res.*, *110*, B12407, doi:10.1029/2005JB003869.

Hetland, E. A., M. Simons, and E. M. Dunham (2010), Post-seismic and interseismic fault creep I: Model description, *Geophys. J. Int.*, *181*, 81–98, doi:10.1111/j.1365-246X.2010.04522.x.

Hirose, T., and T. Shimamoto (2003), Fractal dimension of molten surfaces as a possible parameter to infer the slip-weakening distance of faults from natural pseudotachylytes, *J. Struct. Geol.*, *25*, 1569–1574, doi:10.1016/S0191-8141(03)00009-9.

Holland, T., and R. Powell (1990), An enlarged and updated internally consistent thermodynamic dataset with uncertainties and correlations, *J. Metamorph. Geol.*, *8*, 89–124, doi:10.1111/j.1525-1314.1990.tb00458.x.

Ida, Y. (1972), Cohesive force across the tip of a longitudinal-shear crack and Griffith's specific surface energy, *J. Geophys. Res.*, *77*, 3796–3805, doi:10.1029/JB077i020p03796.

Jeffreys, H. (1942), On the mechanics of faulting, *Geol. Mag.*, *79*, 291–295, doi:10.1017/S0016756800076019.

Lachenbruch, A. H. (1980), Frictional heating, fluid pressure, and the resistance to fault motion, *J. Geophys. Res.*, *85*, 6097–6112, doi:10.1029/JB085iB11p06097.

Matsu'ura, M., H. Kataoka, and B. Shibazaki (1992), Slip-dependent friction law and nucleation processes in earthquake rupture, *Tectonophysics*, *211*, 135–148, doi:10.1016/0040-1951(92)90056-C.

McKenzie, D., and J. Brune (1972), Melting on fault planes during large earthquakes, *Geophys. J. R. Astron. Soc.*, *29*, 65–78.

Nielsen, S., G. Di Toro, T. Hirose, and T. Shimamoto (2008), Frictional melt and seismic slip, *J. Geophys. Res.*, *113*, B01308, doi:10.1029/2007JB005122.

Nielsen, S., P. Mosca, G. Giberti, G. Di Toro, T. Hirose, and T. Shimamoto (2010), On the transient behavior of frictional melt during seismic slip, *J. Geophys. Res.*, *115*, B10301, doi:10.1029/2009JB007020.

Noda, H., E. M. Dunham, and J. R. Rice (2009), Earthquake ruptures with thermal weakening and the operation of major faults at low overall stress levels, *J. Geophys. Res.*, *114*, B07302, doi:10.1029/2008JB006143.

Ohnaka, M., and T. Yamashita (1989), A cohesive zone model for dynamic shear faulting based on experimentally inferred constitutive relation and strong motion source parameters, *J. Geophys. Res.*, *94*, 4089–4104, doi:10.1029/JB094iB04p04089.

Otsuki, K., N. Monzawa, and T. Nagase (2003), Fluidization and melting of fault gouge during seismic slip: Identification in the Nojima fault zone and implications for focal earthquake mechanisms, *J. Geophys. Res.*, *108*(B4), 2192, doi:10.1029/2001JB001711.

Pittarello, L., G. Di Toro, A. Bizzarri, G. Pennacchioni, J. Hadizadeh, and M. Cocco (2008), Energy partitioning during seismic slip in pseudotachylyte-bearing faults (Gole Larghe Fault, Adamello, Italy), *Earth Planet. Sci. Lett.*, *269*, 131–139, doi:10.1016/j.epsl.2008.01.052.

Rempel, A., and J. Rice (2006), Thermal pressurization and onset of melting in fault zones, *J. Geophys. Res.*, *111*, B09314, doi:10.1029/2006JB004314.

Screen, J. A., and I. Simmonds (2010), The central role of diminishing sea ice in recent Arctic temperature amplification, *Nature*, *464*, 1334–1337, doi:10.1038/nature09051.

Shaw, H. (1972), Viscosities of magmatic silicate liquids: An empirical method of prediction, *Am. J. Sci.*, *272*, 870–893, doi:10.2475/ajs.272.9.870.

Sibson, R. H. (1975), Generation of pseudotachylytes by ancient seismic fault, *Geophys. J. R. Astron. Soc.*, *43*, 775–794.

Sibson, R. H. (1977), Kinetic shear resistance, fluid pressures and radiation efficiency during seismic faulting, *Pure Appl. Geophys.*, *115*, 387–400, doi:10.1007/BF01637116.

Sibson, R. H. (2003), Thickness of the seismic slip zone, *Bull. Seismol. Soc. Am.*, *93*(3), 1169–1178, doi:10.1785/0120020061.

Sirono, S., K. Satomi, and S. Watanabe (2006), Numerical simulations of frictional melting: Small dependence of shear stress drop on viscosity parameters, *J. Geophys. Res.*, *111*, B06309, doi:10.1029/2005JB003858.

Sone, H., and T. Shimamoto (2009), Frictional resistance of faults during accelerating and decelerating earthquake slip, *Nat. Geosci.*, *2*, 705–708, doi:10.1038/ngeo637.

Spray, J. (1992), A physical basis for the frictional melting of some rock forming minerals, *Tectonophysics*, *204*, 205–221.

Spray, J. (1995), Pseudotachylyte controversy: Fact or friction?, *Geology*, *23*, 1119–1122, doi:10.1130/0091-7613(1995)023<1119:PCFOF>2.3.CO;2.

Swanson, M. P. (1992), Fault structure, wear mechanisms and rupture processes in pseudotachylyte generation, *Tectonophysics*, *204*, 223–242, doi:10.1016/0040-1951(92)90309-T.

Tsutsumi, A., and T. Shimamoto (1997), High-velocity frictional properties of gabbro, *Geophys. Res. Lett.*, *24*, 699–702, doi:10.1029/97GL00503.

A. Bizzarri, Istituto Nazionale di Geofisica e Vulcanologia, Sezione di Bologna, Via Donato Creti, 12, Bologna I-40128, Italy. (bizzarri@bo.ingv.it)